Molecular Therapy
Original Article

Olaparib Suppresses MDSC Recruitment via SDF1α/CXCR4 Axis to Improve the Anti-tumor Efficacy of CAR-T Cells on Breast Cancer in Mice

Ruixin Sun,[1,4] Hong Luo,[1,2,4] Jingwen Su,[1] Shengmeng Di,[1] Min Zhou,[1] Bizhi Shi,[1] Yansha Sun,[1] Guoxiu Du,[3] Honghong Zhang,[3] Hua Jiang,[1] and Zonghai Li[1,2,3]

[1]State Key Laboratory of Oncogenes and Related Genes, Shanghai Cancer Institute, Renji Hospital, Shanghai Jiaotong University School of Medicine, Shanghai 200032, China; [2]State Key Laboratory of Oncogenes and Related Genes, Renji Hospital, School of Biomedical Engineering, Shanghai Jiao Tong University, Shanghai 200032, China; [3]CARsgen Therapeutics, Shanghai 200032, China

A hostile tumor microenvironment is one of the major obstacles for the efficacy of chimeric antigen receptor modified T (CAR-T) cells, and combination treatment might be a potential way to overcome this obstacle. Poly(ADP-ribose) polymerase inhibitor (PARPi) has demonstrated tremendous potential in breast cancer. In this study, we explored the possible combination of the PAPRi olaparib with EGFR*v*III-targeted CAR (806-28Z CAR) T cells in immunocompetent mouse models of breast cancer. The results indicated that the administration of olaparib could significantly enhance the efficacy of 806-28Z CAR-T cells *in vivo*. Interestingly, we observed that olaparib could suppress myeloid-derived suppressor cell (MDSC) migration and promote the survival of $CD8^+$ T cells in tumor tissue. Mechanistically, olaparib was shown to reduce the expression of SDF1α released from cancer-associated fibroblasts (CAFs) and thereby decreased MDSC migration through CXCR4. Taken together, this study demonstrated that olaparib could increase the antitumor activities of CAR-T cell therapy at least partially through inhibiting MDSC migration via the SDF1α/CXCR4 axis. These findings uncover a novel mechanism of PARPi function and provide additional mechanistic rationale for combining PARPi with CAR-T cells for the treatment of breast cancer.

INTRODUCTION

Breast cancer remains the leading cause of death from malignant tumors among women, despite significant advances in surgery, chemotherapy, radiotherapy, endocrine therapy, and now molecular-targeted therapy. Chimeric antigen receptors (CARs) are engineered receptors with an extracellular, antigen-specific, single-chain variable fragment (scFv) fused with intracellular T cell-activating and costimulatory signaling domains. T cells isolated from patients are activated and genetically engineered to express CARs to mediate non-major histocompatibility complex (MHC)-restricted killing of tumor cells. To date, CAR-T cells are effective in the treatment of several hematologic malignances and are being actively investigated for the treatment of solid tumors, such as breast cancer.[1–4] However, the efficacy in solid tumor is still far from proven. The immunosuppressive microenvironment within solid tumors may contribute to the non-satisfactory performance of CAR-T cells in solid tumors. Immune cells, such as macrophages, dendritic cells (DCs), and myeloid-derived suppressor cells (MDSCs), are an important component of the tumor microenvironment that greatly impact tumor development and therapeutic outcomes.[5] To overcome this obstacle in solid tumors, several corresponding strategies were proposed, including the combination with immune-regulating agents.[6,7]

Poly(ADP-ribose) polymerase (PARP) is identified as a key molecule in the repair of DNA single-strand breaks (SSBs).[8] Inactivation of SSB repair by PARP inhibitor (PARPi) during S-phase induces DNA double-strand breaks (DSBs) and may thus confer synthetic lethality to cells with defective homology-directed DSB repair.[9] PARPi has been shown to be an effective therapeutic strategy against tumors associated with germline mutation in double-strand DNA repair genes by inducing synthetic lethality.[10] In recent years, PARPi has demonstrated tremendous potential in breast cancer, and several active clinical trials are evaluating PARPi-containing combination therapies for advanced breast cancer. Olaparib is the most widely studied third-generation PARPi in clinical practice. It is a potent PARP1 inhibitor that kills tumor cells mainly by participating in DNA defect repair pathways. Veliparib is a small molecule oral PARPi that entered clinical trials in 2006 and is currently used primarily in combination with various chemotherapeutic drugs.[11,12] It has been reported that olaparib could induce $CD8^+$ T cell infiltration

Received 7 April 2020; accepted 22 September 2020;
https://doi.org/10.1016/j.ymthe.2020.09.034.

[4]These authors contributed equally to this work

Correspondence: Zonghai Li, State Key Laboratory of Oncogenes and Related Genes, Shanghai Cancer Institute, Renji Hospital, Shanghai Jiaotong University School of Medicine, Shanghai 200032, China.
E-mail: zonghaili@shsmu.edu.cn
Correspondence: Hua Jiang, State Key Laboratory of Oncogenes and Related Genes, Shanghai Cancer Institute, Renji Hospital, Shanghai Jiaotong University School of Medicine, Shanghai 200032, China.
E-mail: jianghuapy@163.com

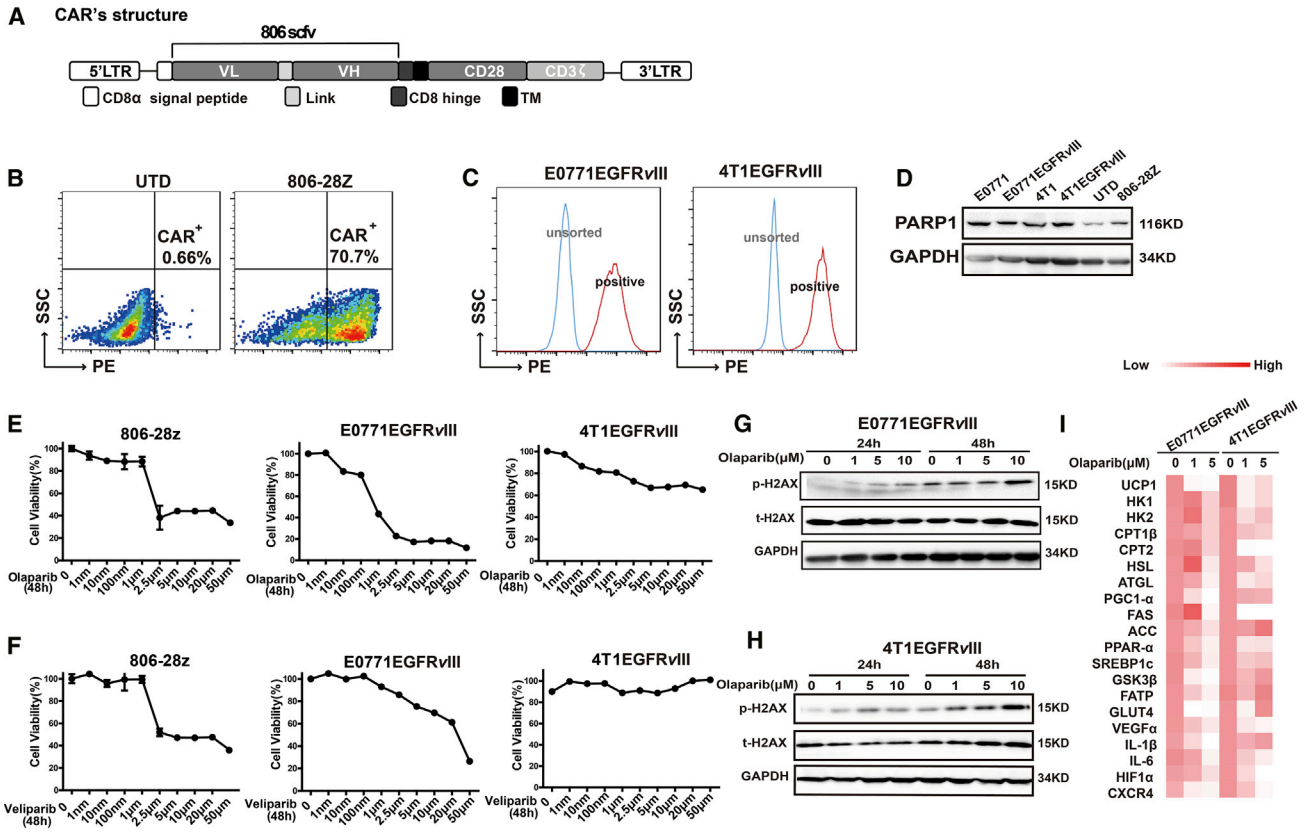

Figure 1. Effects of Olaparib on Mouse Breast Cancer Cells and CAR-T Cells *In Vitro*

(A) The construction of 806-28Z CAR-T cells. This construct includes an extracellular region of antigen recognition, a transmembrane domain (TM), an intracellular region of mouse CD28 costimulatory molecules, and a mouse CD3-ζ chain. (B) The transduction efficiency of 806-28Z CAR on splenic T cells derived from C57BL/6 was determined by flow cytometry. UTD cells served as negative controls. (C) The establishment of 4T1EGFRvIII cells and E0771EGFRvIII cells. (D) Western blot of PARP1 expression in tumor cells and T cells. Glyceraldehyde 3-phosphate dehydrogenase (GAPDH) served as a loading control. (E and F) The cytotoxicity of (E) olaparib or (F) veliparib to CAR-T cells and tumor cells was shown after treatment with indicated concentrations of olaparib or veliparib for 48 h. (G and H) More pronounced DNA breaks in chromosome bridges caused by olaparib were observed in a dose-dependent manner. (G) E0771EGFRvIII cells and (H) 4T1EGFRvIII cells were treated with 0, 1μM, 5μM, or 10μM olaparib for 24 or 48 h. The expressions of p-H2AX (γ-H2AX), H2AX, and GAPDH were determined by western blot. (I) The qRT-PCR analysis showed energy metabolism-related genes expression in EGFRvIII-positive tumor cells after olaparib treatment for 48 h.

and activation in breast cancer and inhibit angiogenesis.[13,14] These findings provide a rationale for combining PARPi with immunotherapies, such as CAR-T cells, for the treatment of breast cancer.

EGFR and EGFR*v*III, the most common EGFR mutant forms with constitutively activated kinase domain, can promote tumor cells proliferation, invasion, and tumor microenvironment angiogenesis. EGFR*v*III has been reported to be expressed in various human cancers, including breast cancer, but has not been detected in normal adult human tissue.[15] EGFR*v*III expression has been detected in approximately 5% of primary breast cancer cases and contributes to cancer stem cell phenotypes in invasive breast carcinomas.[16] EGFR*v*III has also been found in circulating breast cancer cells and correlated with breast cancer metastasis.[17] In our previous studies, we have generated EGFR*v*III-targeting CAR-T cells and defined that EGFR*v*III has an anti-tumor effect, especially in breast cancer.[10,18,19]

In this study, we explored the possible combination of olaparib with EGFR*v*III-targeting CAR (806-28Z CAR) T cells in immunocompetent mouse models of breast cancer. Our results demonstrated that olaparib might suppress the recruitment of MDSCs to improve the immunosuppressive microenvironment, which contributes to the infiltration and survival of CAR-T cells. These findings uncover a novel mechanism of PARPi and provide an additional mechanistic rationale for combining PARPi with CAR-T therapy for the treatment of breast cancer.

RESULTS

Effects of Olaparib on Mouse Breast Cancer Cells and CAR-T Cells *In Vitro*

We constructed a retroviral vector encoding 806-28Z CAR, which was composed of an extracellular scFv derived from 806 antibody linked through a hinge region to a mouse CD8 transmembrane region and a mouse CD28 intracellular signaling domain and CD3-ζ chains

(Figure 1A). The transduction efficiency of 806-28Z CAR (T cells from C57BL/6 mice) was 70.7% (Figure 1B) and 52.9% (T cells from BALB/c mice) (Figure S1A), which was determined by flow cytometry. EGFR*v*III-positive E0771 and 4T1 cells were sorted out successfully (Figure 1C). *BRCA1/2* defects have therapeutic implications, as it confers the sensitivity to platinum-based drugs and PAPRi.[20] The mRNA expressions of *BRCA1* and *BRCA2* in EGFR*v*III-positive tumor cells were observed, which were much higher in 4T1EGFR*v*III cells than in E0771EGFR*v*III cells (Figure S1B). In this study, we evaluated the cytotoxicity of PARPi on the two mouse breast cancer cells and CAR-T cells with different *BRCA1/2* expression. Expression of PARP1 was detected in mouse breast cancer cells, mouse T cells, and CAR-T cells (Figure 1D). Since the homology of PARP1 protein in mouse and human cells reaches 99.9%, and the binding site of PARPi is consistent in mouse and human cells, the PARPi could be used in mouse cells. In this study, we chose the two main PARPis, olaparib and veliparib, to explore the impact of PARPis on different cells. According to proliferation analysis, olaparib presented better cytotoxicity in EGFR*v*III-positive cells than veliparib (Figures 1E and 1F), and olaparib could also suppress the proliferation of CAR-T cells when the concentration of olaparib reached 2.5 μM and above (Figures 1E and 1F). Further, more pronounced DNA breaks in chromosome bridges caused by olaparib were observed in a dose-dependent manner in mouse breast cancer cells as judged by *p*-H2AX (γ-H2AX) (Figures 1G and 1H). Olaparib treatment could induce DNA damage even at 1 μM concentration (Figures 1G and 1H). Moreover, EGFR*v*III-positive tumor cells treated with olaparib showed a state of senescence with less cell proliferation, as observed by β-galactosidase staining (Figure S1C), and olaparib exposure resulted in a significant reduction of energy metabolism-related gene expression (Figure 1I). These alterations were attributed to a reduction in proliferation of mouse breast cancer cells treated with olaparib.

The exhaustion markers of mouse CAR-T cells were then tested. No significant differences appeared in the expression of T cell exhaustion-related proteins (PD1, TIM3, and LAG3) of CAR-T cells treated with olaparib (Figure S1D). Further, olaparib treatment could induce more CAR-T cell apoptosis ($p < 0.05$; Figure S1E), and the percentages of central memory T cell (T_{cm}) ($CD8^+CD44^+CD62L^+$) cells were elevated in olaparib-treated CAR-T cells ($p < 0.01$; Figure S1F), suggesting the possible role of olaparib in improving cell persistence *in vivo*.

Olaparib Enhances the Antigen-Induced CAR-T Cell Responses

In Vitro

Due to the impact of olaparib on the proliferation of CAR-T cells, target cells were pretreated with 0, 1 μM, or 5 μM olaparib for 24 h. Then the medium of the co-culture of effector and target cells was added with or without olaparib 1 μM or 5 μM (Figure 2A). Murine CAR-T cells showed significant specific cytolysis activity against EGFR*v*III-positive tumor cells but not antigen-negative tumor cells (Figures 2B and 2C). Significantly higher specific lysis of the target cells could be detected at a 3:1 effector-to-target (E/T) ratio compared to a 1:3 or 1:1 E/T ratio (Figure 2C). The cytotoxic activity of CAR-T cells after olaparib exposure was enhanced at a 1:3 E/T ratio in the co-culture system (Figure 2C). Furthermore, cytokine secretion by CAR-T cells in response to antigen stimulation was also measured in the presence of different concentrations of olaparib. Increased interferon-γ (IFN-γ) production by CAR-T cells was observed in the presence of olaparib in E0771EGFR*v*III cells (Figure 2D). However, there were no differences of interleukin-2 (IL-2) and granzyme B secretion by CAR-T cells in either the olaparib pretreatment or the treatment group (Figure 2D). The phenotype of CAR-T cells in response to antigen stimulation was then evaluated. Stimulated with EGFR*v*III-positive tumor cells, there were no significant differences in the percentages of $CD8^+$ T cells, T_{cm} cells, and the expression of T cell exhaustion-related protein of CAR-T cells in each treatment group (Figures S2A–S2D). Of note, with olaparib exposure, more apoptosis and less proliferation of CAR-T cells were observed in the olaparib and CAR-T cell co-culture system. However, in olaparib pretreatment conditions, the apoptosis and proliferation of CAR-T cells were almost not changed (Figures 2E and 2F). Moreover, the combination of olaparib with CAR-T cells could induce significant tumor cell apoptosis (Figure 2G).

Olaparib Enhances the Anti-Tumor Activity of CAR-T Cells

In Vivo

To address whether olaparib could enhance the anti-tumor activities of CAR-T cells, mice bearing EGFR*v*III-positive tumor xenografts were established (Figures 3A and 4A). The mice were administered olaparib at a dose of 10, 50, or 100 mg/kg/day from day 14 to 24 and treated with CAR-T cells on day 21 after tumor cell inoculation (Figure S3A). The results showed that a 50 mg/kg dose of olaparib could significantly enhance the tumor-suppression activity of CAR-T cell, as shown by the delayed tumor growth and lighter tumor weight (Figures S3B and S3C). Meanwhile, we did not find any severe toxicity on mice treated with CAR-T cells or olaparib *in vivo*. No morphological abnormality appeared in the H&E staining of the tissue sections from heart, liver, spleen, lung, and kidney (Figure S3D). Therefore, in the following experiments *in vivo*, mice bearing EGFR*v*III-positive tumors were administered olaparib at a dose of 50 mg/kg/day to combine with CAR-T cells (Figures 3A and 4A).

Tumor growth and body weight of mice were observed for 35 days after tumor cell inoculation (Figures 3B, 3C, 4B, and 4C). The body weight of mice showed no significant difference in all groups, suggesting no severe toxicity caused by CAR-T and olaparib treatment (Figures 3C and 4C). Single administration of olaparib had no inhibitory effect on tumor growth, whereas the tumor-suppression activities were significantly improved after combining with CAR-T cells. Compared with single CAR-T cells or olaparib treatment groups in E0771EGFR*v*III tumor xenografts, CAR-T cell (2×10^6 and 5×10^6) treatment in combination with olaparib (50 mg/kg) led to stronger tumor growth inhibition ($p < 0.01$; Figure 3B). In 4T1EGFR*v*III tumor xenografts, CAR-T cell (5×10^6) treatment in combination with olaparib (50 mg/kg) also significantly suppressed the tumor growth compared with single CAR-T cells or olaparib treatment

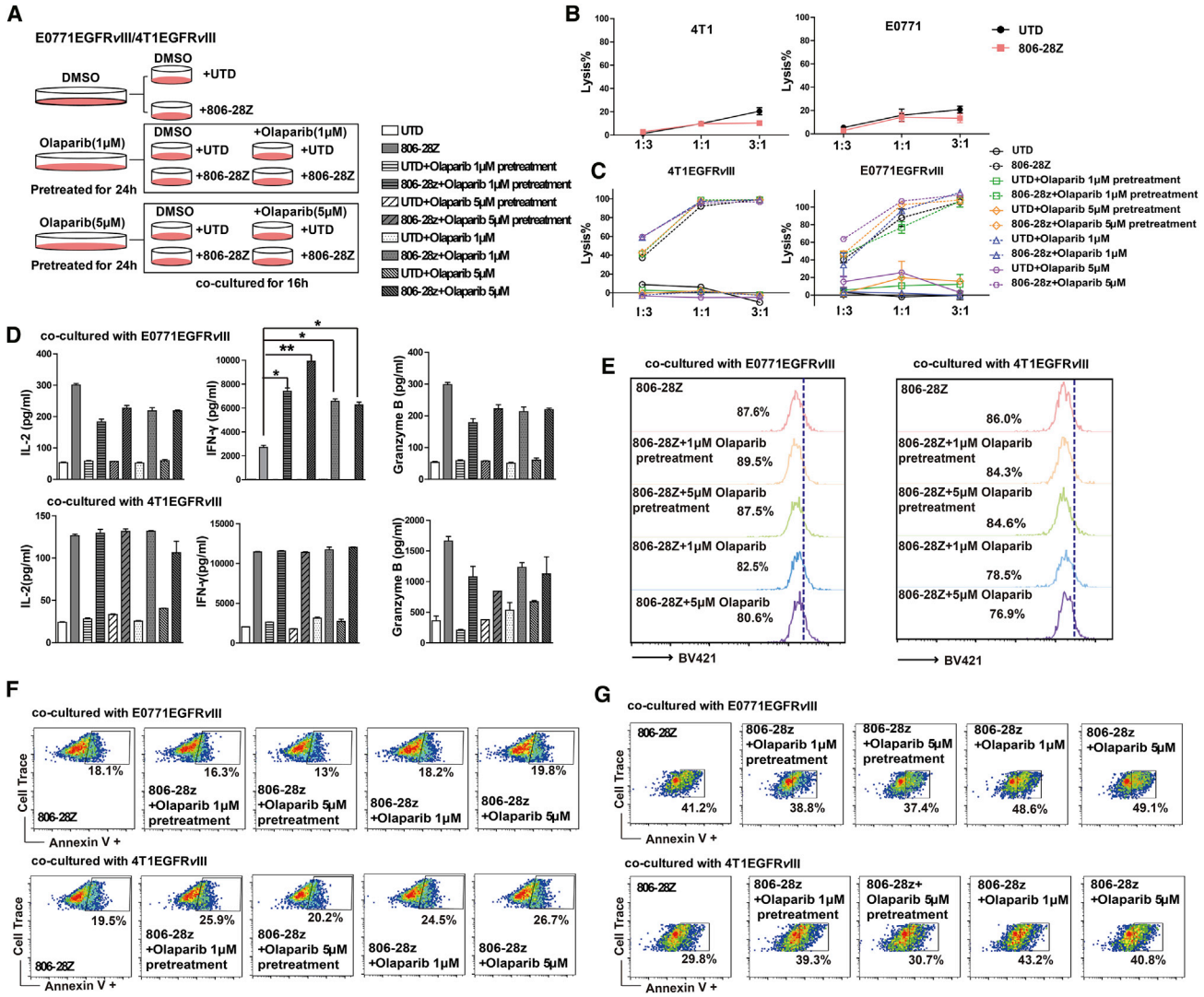

Figure 2. Olaparib Enhances the Antigen-Induced CAR-T Cell Responses *In Vitro*

(A) Schematic diagram of cytotoxic activities of CAR-T cells combined with olaparib. Target cells were pre-treated with 0, 1 μM, or 5 μM olaparib for 24 h. Then the medium of the co-culture system was added with or without olaparib (1 μM or 5 μM) in E-plate at 37°C for 18 h. (B) *In vitro* cytotoxic activities of CAR-T cells on EGFRvIII-negative tumor cells. (C) The cytotoxicity analysis after incubation of EGFRvIII-positive tumor cells and CAR-T cells at the three E/T ratios in different olaparib treatment groups. (D) The levels of IFN-γ, IL-2, and granzyme B in the co-cultured supernatants were determined by ELISA. (E) The number of gated cells indicates the dividing cell population of CAR-T cells. EGFRvIII-positive tumor cells were pre-treated with or without various concentrations of olaparib for 24 h. 1×10^5 CellTrace-labeled CAR-T cells were incubated with 1×10^5 EGFRvIII-positive tumor cells at a 1:1 E/T ratio in the presence of various concentrations of olaparib for 24 h. (F and G) The representative flow cytometry plots showing the frequencies of Annexin V^+ (F) CAR-T cells and (G) EGFRvIII-positive tumor cells. All data are presented as the mean ± SEM of triplicate experiments. *$p < 0.05$, **$p < 0.01$.

($p < 0.05$; Figure 4B). Tumor inhibition rates and tumor weights were measured and were in accordance with tumor volumes (Figures 3D, 3E, 4D, and 4E). DNA copy numbers were more significantly elevated in the CAR-T cells in combination with the olaparib (50 mg/kg) group than those of other groups (Figures 3F and 4F). Compared with single CAR-T cell treatment, CAR-T cells in combination with olaparib treatment showed more $CD8^+$ T cells and fewer $CD31^+$ cells in tumor tissue by immunohistochemical (IHC) staining, whereas the $CD4^+$T cells in each group showed no differences (Figures 3J, 3K, 4J, and 4K). These data suggested that combination with olaparib treatment could improve the anti-tumor efficacy of CAR-T cell therapy in immunocompetent mouse models.

Olaparib Decreased MDSC Recruitment in Tumor Tissue of Tumor-Bearing Mice

MDSCs have emerged as important contributors to solid tumor immune evasion.[21] In our study, the infiltration of $CD45^+$ immune cells and MDSCs was analyzed via flow cytometry on day 28. Large amounts of MDSCs were detected in the tumor tissue of EGFRvIII-positive tumor-bearing mice (Figures 3G and 4G). However, after

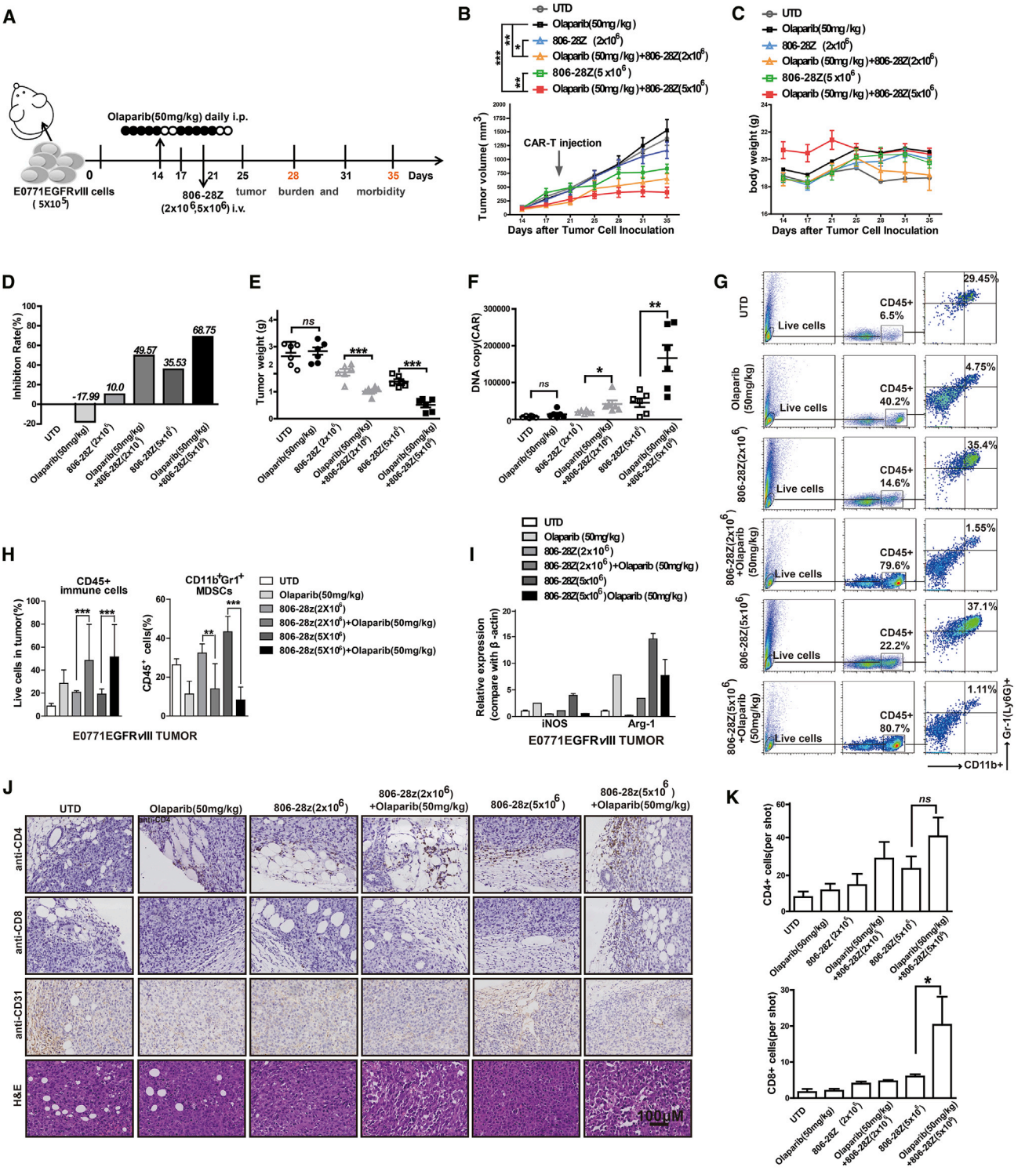

Figure 3. Olaparib Enhances the Anti-tumor Activity of CAR-T Cells in Mice Bearing E0771EGFRvIII Tumor Cells

(A) *In vivo* experimental design. E0771EGFRvIII tumor cells (5×10^5) were *in situ* inoculated into C57BL/6 mice and allowed to establish for 14 days. Mice were assigned to six experimental groups and indicated PBS or olaparib (50 mg/kg) was administered via intraperitoneal injection for 10 days. CAR-T cells were injected intravenously (i.v.) on day 21. (B–E) Tumor growth (B), body weight (C), tumor inhibition rate (D), and tumor weight (E) of each treatment group (n = 6). (F) CAR copy number in genomic DNA of residual

(legend continued on next page)

olaparib treatment, the ratio of $CD45^+$ immune cells in tumor tissue of EGFR*v*III-positive tumor-bearing mice was increased, whereas the ratio of MDSCs was significantly decreased (Figures 3G, 3H, 4G, and 4H). L-Arg (L-arginase) is depleted by inducible nitric oxide synthase (iNOS), and Arg-1 is produced by MDSCs, leading to the depression of T cells.[22] The mRNA expressions of Arg-1 and iNOS were increased, which were the related markers of MDSCs (Figures 3I and 4I). It has been reported that olaparib could induce the recruitment of $CD8^+$ T cells into tumor tissue.[13] The results of IHC staining indicated that there was more infiltration of $CD8^+$ T cells in tumor tissue in the combination treatment group than those of the single CAR-T cell treatment group (Figures 3J, 3K, 4J, and 4K). Previously, we observed that MDSCs could suppress mouse T cell proliferation.[19] To evaluate the contribution of MDSCs on the survival of CAR-T cells, MDSCs were isolated from the bone marrow of C57BL/6 mice and co-cultured with CAR-T cells for 24 h (Figures 5A and 5B; Figure S4A). As shown in Figure 5B, the $CD8^+$T cells presented more cell apoptosis when co-cultured with MDSCs, suggesting that the decreased presence of MDSCs should promote the survival of $CD8^+$ T cells in tumor tissue in the combination treatment group. Moreover, MDSCs could inhibit the lytic activity of CAR-T cells in a dose-dependent manner (Figure S4B). To exclude the direct toxic effect of olaparib on MDSCs, MDSCs were treated with different doses of olaparib *in vitro*. The cell proliferation results showed that olaparib had almost no direct toxic effects on MDSCs (Figure S4C). Further, the toxic effect of olaparib on MDSCs *in vivo* was also investigated (Figure S5A). The results showed that, compared with the control group, no significant differences of MDSCs were observed in blood, spleen, and bone marrow from mice bearing EGFR*v*III-positive tumor xenografts treated with different doses of olaparib (Figures S5B–S5G). These results suggested that olaparib improving the anti-tumor effects of CAR-T cells was attributed to the reduction of MDSC recruitment in tumor tissue of tumor-bearing mice.

Olaparib Induced SDF1α Downregulation in CAFs

The tumor microenvironment is composed of extracellular matrix (ECM) and non-malignant stromal cells, including fibroblasts, pericytes, immune cells, and endothelial cells.[23] Cancer-associated fibroblasts (CAFs) are the main cell types constituting the tumor stroma of breast cancer.[23] In this study, the expression of CAFs was examined by immunostaining, and large number of CAFs were observed in tumor tissue of EGFR*v*III-positive tumor-bearing mice (Figure S6A). MDSCs could be recruited into tumor tissue by a variety of chemokines. To determine the key chemokines relevant to olaparib-reduced recruitment of MDSCs, mRNA levels of chemokines and cytokines were detected in tumor tissue from EGFR*v*III-positive tumor-bearing mice (Figures S6B and S6C). The stromal cell-derived factor 1α (SDF1α), also known as CXCL12, was produced in different cell types, including stromal cells such as CAFs. A previous study reported that CAFs could promote the recruitment of MDSCs via the SDF1α/CXCR4 axis in tumor tissue, which led to tumor growth.[24] The SDF1α/CXCR4 axis also participates in promoting the proliferation and migration of breast cancer cells.[25,26] In this study, our results showed that the protein expression of both SDF1α and CXCR4 was decreased with olaparib treatment in the tumor tissue of EGFR*v*III-positive tumor-bearing mice (Figures 5C–5F). In addition, tumor-derived CAF cells were isolated from mammary tissues of mice bearing EGFR*v*III-positive tumor xenografts (Figure S6D). There was almost no difference of SDF1α expression in tumor tissue and tumor-derived CAFs (Figure S6E). These results suggested that SDF1α in tumor tissue was mainly derived from CAFs.

Next, to determine the effect of olaparib on the SDF1α expression in CAFs, mouse fibroblast NIH 3T3 cells were first induced into CAFs by starvation and transforming growth factor β (TGF-β) treatment according to the previous report.[27] As shown in Figure 5G, the protein level of α-smooth muscle actin (α-SMA), a marker of CAFs, was significantly increased in induced NIH 3T3 cells. We know that the tumor environment is hypoxic, and in order to imitate the hypoxic environment, EGFR*v*III-positive tumor cells and CAFs were cultured in the absence or presence of 1% O_2 conditions. The mRNA expressions of a variety of chemokines were increased under hypoxic conditions, including SDF1α (Figure S6F). The protein expression of CXCR4 in the EGFR*v*III-positive tumor cells and SDF1α in CAFs were all downregulated after 48 h treatment of olaparib under hypoxic conditions (Figure 5H–5K).

Olaparib Reduced the Recruitment of MDSCs in an SDF1α-Dependent Manner

It has been reported that CAFs could produce key growth factors and cytokines to recruit immune cells, especially immunosuppressive cells, into the tumor stroma.[21] High levels of pro-inflammatory cytokines and chemokines were detected in CAFs (Figure 6A). The mRNA expression of SDF1α was significantly decreased in CAFs with olaparib treatment (Figure 6B). To determine whether the olaparib-reduced SDF1α in CAFs contributed to less recruitment of MDSCs, MDSCs were Transwell cultured in the upper chamber, with the cell culture supernatant of CAFs treated with different concentrations of olaparib (0, 1 μM, or 5 μM) in the lower compartment (Figure 6C). Less migration of MDSCs was detected in the cell culture supernatant of CAFs treated with olaparib group (Figure S7A). MDSCs treated with or without olaparib were added in the upper chamber, while the cell culture supernatant of CAFs was in the lower chamber of the Transwell co-culture system. Less migration of MDSCs was detected in the olaparib treatment group (Figure S7B). Then, we evaluated the impact of olaparib on CXCR4 expression of MDSCs. The CXCR4 expression on the cell surface of

tumors 10 days after therapy was measured by qRT-PCR (TaqMan probe). (G and H) The representative flow cytometry plots showing the (G) frequencies and (H) quantitations of tumor-infiltrating $CD45^+$ immune cells and MDSCs of each treatment group. (I) The mRNA expression of iNOS and Arg-1 in E0771EGFRvIII tumor tissue of mice. (J and K) The tumor tissues from mice of each treatment group were immumostained with anti-CD4, anti-CD8, or anti-CD31 Ab and H&E staining. (J) The representative immunostaining images (K) and quantifification of CD4+ ,CD8+, and CD31+ cells in tumor tissues from each treatment group. The images were obtained under original magnification 200×. Scale bars, 100 μm. All data are presented as the mean ± SEM of triplicate experiments. *$p < 0.05$, **$p < 0.01$, ***$p < 0.001$.

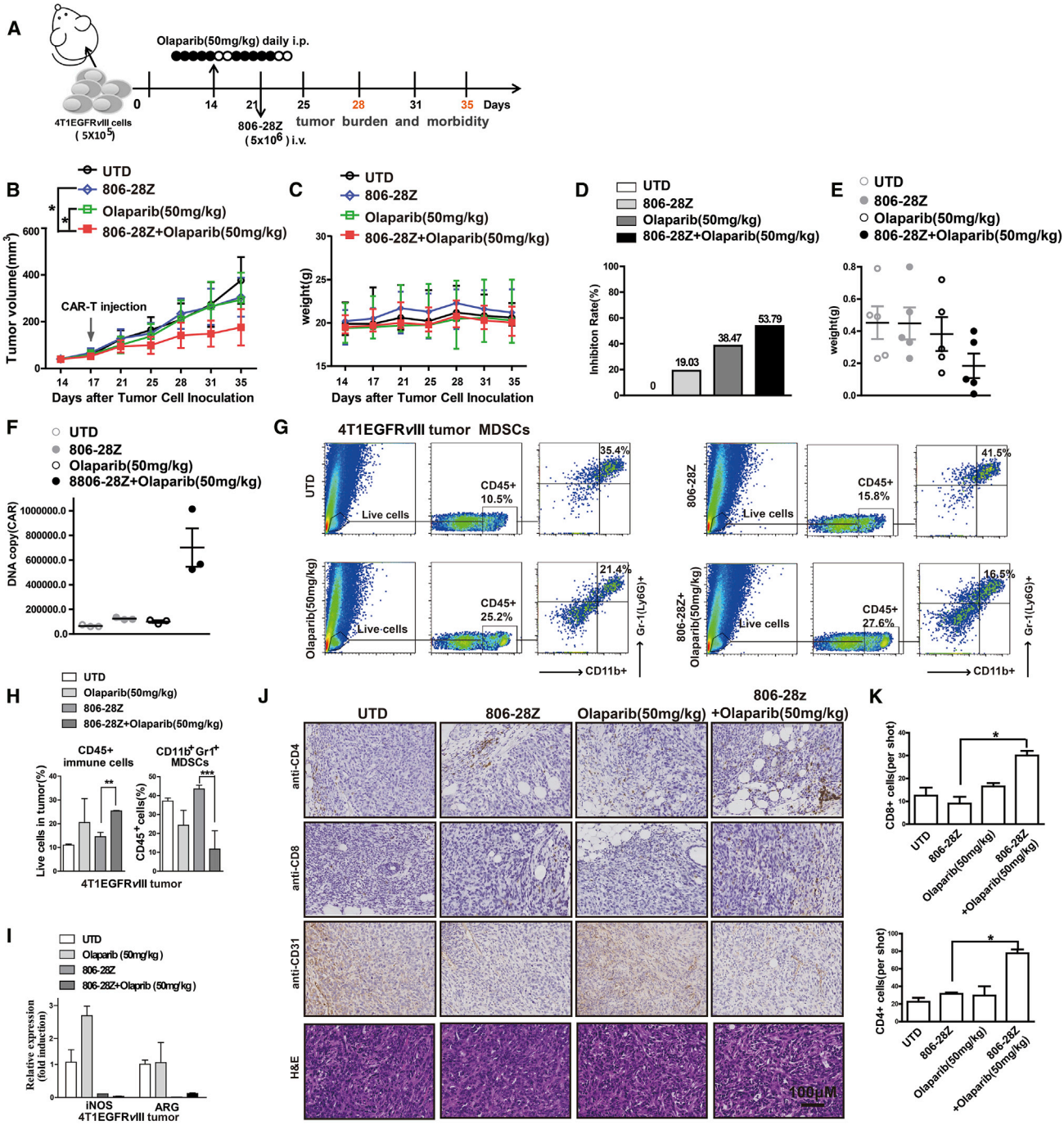

Figure 4. Olaparib Enhances the Anti-tumor Activity of CAR-T Cells in Mice Bearing 4T1EGFRvIII Tumor Cells

(A) *In vivo* experimental design. 4T1EGFRvIII tumor cells (5×10^5) were *in situ* inoculated into BABL/c mice and allowed to establish for 14 days. Mice were assigned to four experimental groups and PBS or olaparib (50 mg/kg) was administered via intraperitoneal injection for 10 days. CAR-T cells were injected i.v. on day 21. (B–E) Tumor growth (B), body weight (C), tumor inhibition rate (D), and tumor weight (E) of each treatment group (n = 6). (F) CAR copy number in genomic DNA of residual tumors 10 days after therapy were measured by qRT-PCR (TaqMan probe). (G and H) The representative flow cytometry plots showing the (G) frequencies and (H) quantitations of tumor-infiltrating $CD45^+$ immune cells and MDSCs of each treatment group. (I) The mRNA expression of iNOS and Arg-1 in 4T1EGFRvIII tumor tissue of mice. (J and K) The sections of formalin-fixed, paraffin-embedded tumor tissue from mice of each group were immunostained with anti-CD4, anti-CD8, or anti-CD31 Ab and H&E staining. The images were obtained under original magnification 200×. Scale bars, 100 μm. All data are presented as the mean ± SEM of triplicate experiments. *$p < 0.05$, **$p < 0.01$, ***$p < 0.001$.

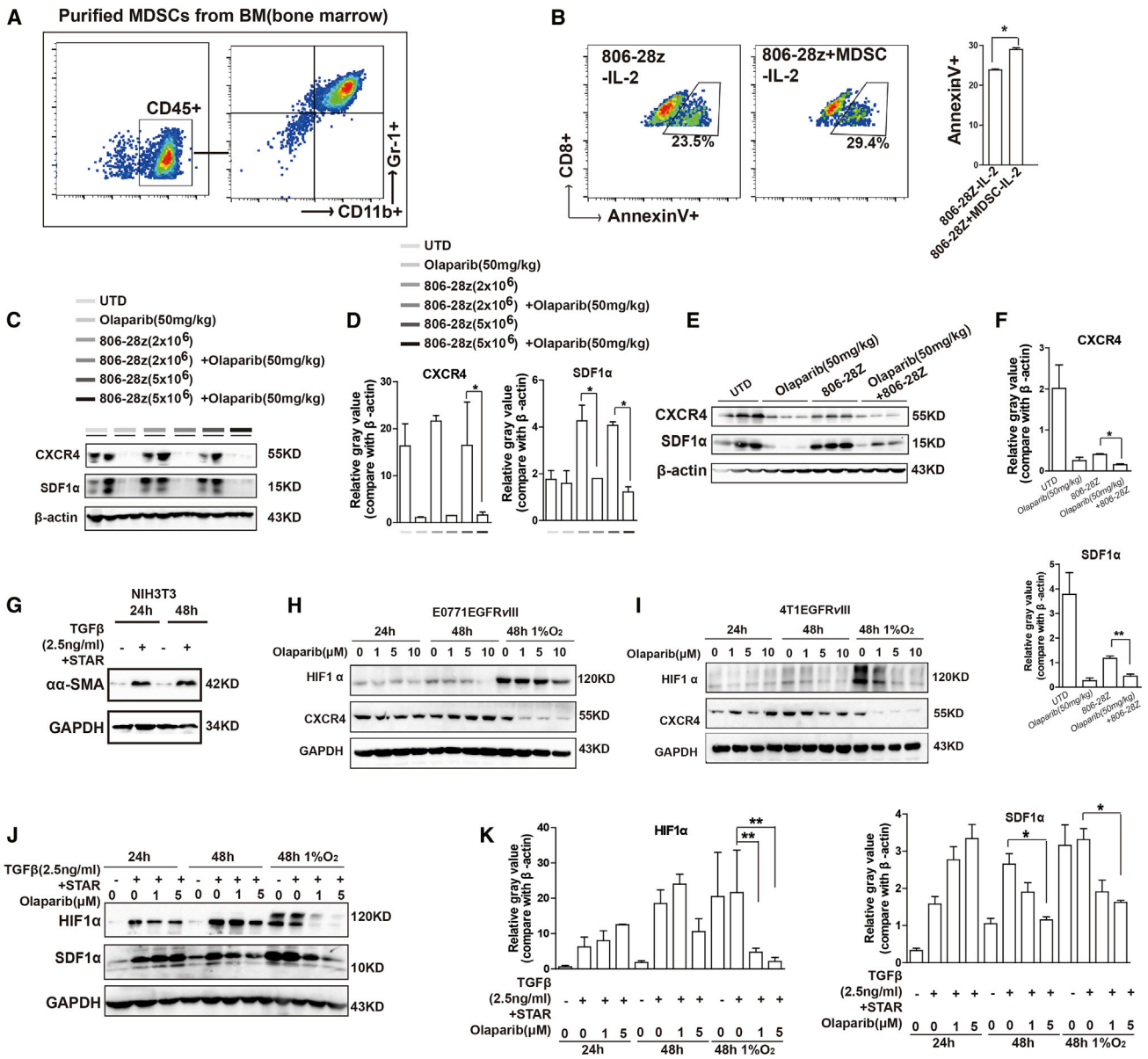

Figure 5. Olaparib Decreased MDSC Recruitment in Tumor Tissue of Tumor-Bearing Mice

(A) Representative flow cytometry plots showing the frequencies of MDSCs ($CD11b^+Gr1^+$ cells) in $CD45^+$ immune cells isolated from bone marrow. (B) The representative flow cytometry plots and quantification results showed the frequencies of Annexin V^+ $CD8^+$ cells in CAR-T cells after co-culture with MDSCs without IL-2 in the medium. (C-F) The protein levels of CXCR4 and SDF1α were decreased with olaparib treatment in the tumor tissue of (C and D) E0771EGFRvIII-tumor bearing mice and (E and F) 4T1EGFRvIII-tumor bearing mice from each treatment group. (G) NIH3T3 cells were starved for 24 h and then treated with TGF-β (2.5 ng/mL) for 16 h to acquire the phenotype of CAFs. The expression of α-SMA was increased in TGF-β-induced conditions. (H and I) The expressions of HIF1α and CXCR4 were decreased in (H) E0771EGFRvIII tumor cells and (I) 4T1EGFRvIII tumor cells after 0, 1 μM, 5 μM, or 10 μM olaparib treatment under normal or hypoxic conditions for 24 or 48 h. (J and K) The expressions of HIF1α and SDF1α were decreased in CAFs treated with olaparib (0, 1 μM, or 5 μM) under normal or hypoxia conditions for 24 or 48 h. GAPDH served as a loading control. All data are presented as the mean ± SEM of triplicate experiments. *$p < 0.05$, **$p < 0.01$.

MDSCs from mice bearing EGFRvIII-positive tumor xenografts treated with olaparib decreased in a dose-dependent manner (Figures S7C and S7D). In addition, *in vitro*, the decreased expression of CXCR4 on the cell surface of MDSCs was also observed in the presence of 1 μM olaparib ($p < 0.01$; Figure S7E). These results suggested that the SDF1α/CXCR4 axis played a key role on olaparib-induced reduction of MDSC migration.

The expression of chemokines released by CAFs such as SDF1α, CXCL1, and CCL2 was downregulated with olaparib treatment

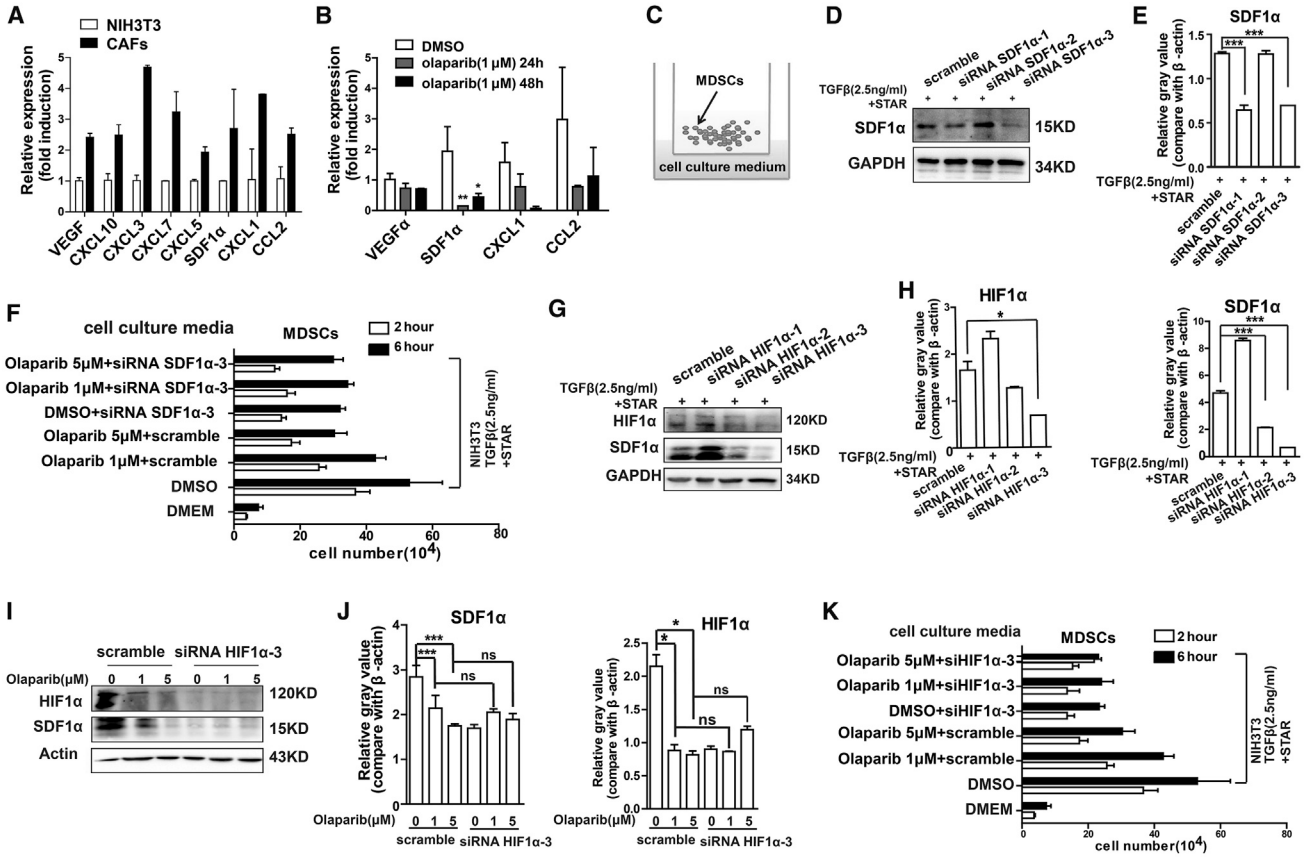

Figure 6. Olaparib Reduced the Recruitment of MDSCs in an SDF1α-Dependent Manner

(A) The mRNA expression of chemokines in NIH 3T3 and CAFs. (B) The mRNA expression of VEGFα, SDF1α, CXCL1, and CCL2 in CAFs treated with DMSO or 1 μM olaparib for 24 h or 48 h. (C) Transwell co-culture of MDSCs with cell culture supernatant of CAFs. 1×10^6 MDSCs were added to the upper chamber and the cell culture supernatant of CAFs was added in the lower chamber. The cell number in the lower chamber was counted at 2 h and 6 h. (D and E) CAFs were transfected with siRNA for 48 h. The expression of SDF1α was determined by western blot, and siRNA-3 of SDF1α could significantly block the SDF1α expression in CAFs. GAPDH served as a loading control. (F) Effects of olaparib and SDF1α on CAF-induced chemotaxis of MDSCs. CAFs were transfected with siRNA SDF1α-3 or scramble, treated with 0, 1 μM, or 5 μM olaparib for 48 h, and then the cell culture supernatant was collected. 1×10^6 MDSCs were added to the upper chamber, and the cell culture supernatant of CAFs was added in the lower chamber. The cell number in the lower chamber was counted at 2 h and 6 h. (G and H) The CAFs were transfected with siRNA of HIF1α for 48 h. The expressions of HIF1α and SDF1α were successfully decreased in CAFs transfected with siRNA-3 of HIF1α. (I and J) CAFs were transfected with siRNA-3 of HIF1α and treated with different concentrations of olaparib for 48 h. The HIF1α and SDF1α levels were decreased with olaparib treatment in control group (scramble).The expression of SDF1α was not changed with olaparib treatment in siRNA-3 of HIF1α transfected group, determined by western blot. (K) Effects of olaparib and HIF1α on CAF-induced chemotaxis of MDSCs. CAFs were transfected with siRNA HIF1α-3 or scramble, treated with 0, 1 μM, or 5 μM olaparib for 48 h and then collected the cell culture supernatant. 1×10^6 MDSCs were added to the upper chamber and the cell culture supernatant of CAFs were added in the lower chamber. The cell number in the lower chamber was counted at 2 h and 6 h. All data are presented as the mean ± SEM of triplicate experiments. ns, not significant; *$p < 0.05$, **$p < 0.01$, ***$p < 0.001$.

(Figure 6B). However, whether SDF1α plays the key role in olaparib-reduced recruitment of MDSCs was not clear. To clarify this, CAFs were transfected with control small interfering RNA (siRNA) (Figure S7F) or the siRNA of SDF1α, and the siRNA-3 of SDF1α could significantly block the SDF1α expression in CAFs ($p < 0.001$; Figures 6D and 6E; Figure S7G). In the Transwell co-culture system, the cell culture supernatants of CAFs transfected with SDF1α siRNA-3 treated with different concentration of olaparib were added in the lower chamber, and MDSCs were Transwell cultured in the upper chamber. The cell culture supernatant of CAFs transfected with siSDF1α-3 induced less MDSC migration compared with the cell culture supernatant of CAFs transfected with scramble siRNA (Figure 6F). However, with decreased expression of SDF1α (CAFs transfected with siSDF1α-3), there was no difference in MDSC migration in the groups of CAFs treated with different concentration of olaparib (Figure 6F), suggesting that the reduced recruitment of MDSCs by olaparib was dependent on SDF1α.

Hypoxia-inducible factor 1α (HIF1α) activates transcription of genes in hypoxic cells. It has been reported that HIF1α levels could be downregulated by olaparib.[28] In this study, the expression of HIF1α decreased in olaparib-treated tumor cells and CAFs in a dose-dependent manner under hypoxic conditions (Figures 5H and 5I). Notably,

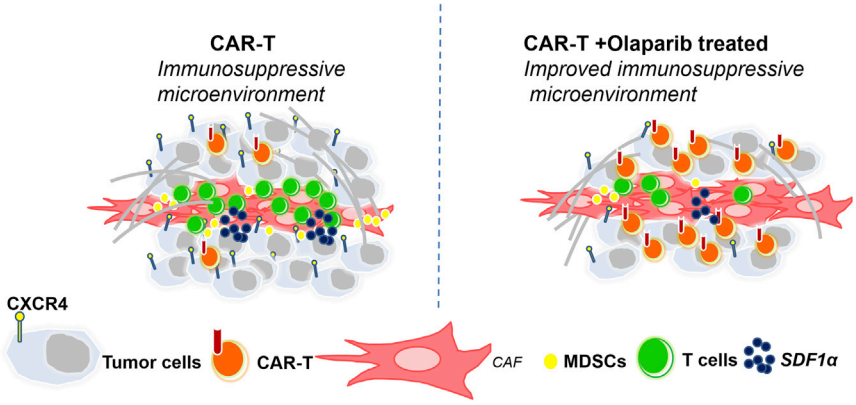

Figure 7. Schema: Olaparib Enhances the Anti-tumor Ability of CAR-T Cells by Suppressing the Infiltration of MDSCs

Left: CAFs have a key role in producing a reactive stroma that frequently perpetuates a tumor-promoting, tissue-repair response. The CAF secretome potentiates tumor angiogenesis through the SDF1α/CXCR4 axis. The CAF secretome could also recruit monocytes from the bone marrow, such as MDSCs, to form a tumor-suppressing microenvironment, which suppresses the infiltration of CAR-T cells. Right: olaparib could suppress the secretion of SDF1α secreted from CAFs, inhibiting the recruiting of MDSCs to the tumor microenvironment. Further, olaparib could also decrease the expression of CXCR4 in tumor cells and MDSCs. With less MDSC recruitment, CAR-T cells could significantly inhibit tumor angiogenesis.

the expression of HIF1α was consistent with the SDF1α expression in CAFs treated with olaparib under hypoxic conditions (Figures 5J and 5K; Figure S7H). To determine whether HIF1α mediates the downregulation of SDF1α, CAFs were transfected with HIF1α siRNA under hypoxic conditions. The expression of HIF1α was successfully decreased in CAFs transfected with the siRNA-3 of HIF1α (Figures 6G and 6H; Figure S7I). Consistently, the expression of SDF1α was also decreased. Furthermore, to confirm whether HIF1α is the key regulator of olaparib-induced SDF1α downregulation in CAFs under hypoxic conditions, CAFs were transfected with HIF1α siRNA-3 or scramble and then treated with or without olaparib under hypoxic conditions. The expression of HIF1α could be suppressed by the siRNA-3 of HIF1α or olaparib treatment in CAFs (Figures 6I and 6J). However, transfection with the siRNA-3 of HIF1α along with olaparib treatment did not induce a synergistic suppression of SDF1α expression (Figures 6I and 6J). Furthermore, with HIF1α knockdown, there were no differences in MDSC migration in the cell culture supernatants from CAFs treated with or without olaparib (Figure 6K). These data demonstrated that olaparib might regulate the SDF1α expression via HIF1α.

DISCUSSION

CAR-T cells have encountered significant challenges for treatment of solid tumors because of their poor trafficking and antigen heterogeneity and the immunosuppressive microenvironment within solid tumors.[29,30] To overcome these obstacles in solid tumors, several corresponding strategies were proposed, including combining CAR-T cells with radiotherapy, chemotherapy, and small molecule inhibitors. In this study, we provided evidence that olaparib, a PARPi, combined with CAR-T cells triggers an anti-tumor immune response with improved recruitment of $CD8^+$ T cells in mouse breast cancer models. Mechanistically, we demonstrated that olaparib might suppress the release of SDF1α in CAFs via HIF1α and further limit the recruitment of MDSCs into tumor tissue, which might promote the survival of $CD8^+$ T cells (Figure 7).

Previously, olaparib was first approved by the US Food and Drug Administration (FDA) in 2014 for the treatment of germline *BRCA1/2*-deficient ovarian cancer.[31] In tumors with no *BRCA1/2* deficiency, a massive dose of olaparib is required for tumor suppression. In this study, the mRNA expressions of *BRCA1* and *BRCA2* were found expressed in EGFR*v*III-positive tumor cells. CAR-T cells combined with olaparib at the dose of 50 mg/kg/day could suppress tumor progress in mice bearing EGFR*v*III-positive cell xenografts. Previous studies showed that the mutation rate of *BRCA1/2* only reaches 12.2% in breast cancers and 25% in triple-negative breast cancers,[32] which limits clinical use of PARPi. However, our data demonstrated that CAR-T cells combined with olaparib might be applied in treating breast cancers without *BRCA1/2* deficiency. Further studies are needed to understand the efficacy of the combination treatment on breast cancers with *BRCA1/2* mutation.

In this study, a high concentration of olaparib was shown to be able to induce CAR-T cell death. Thus, tumor cells were pre-treated with olaparib to reduce the growth-suppression effect of olaparib on CAR-T cells and enhance the cytotoxicity of CAR-T cells *in vitro*. Here, increased IFN-γ produced by CAR-T cells was observed in the presence of olaparib co-cultured with E0771EGFR*v*III cells *in vitro*. However, *in vivo* there were no significant differences of serum IFN-γ in the CAR-T cells treatment group and combination treatment group from mice bearing EGFR*v*III-positive tumor xenografts (data not shown). These results suggested that olaparib might improve IFN-γ secretion in the co-culture system *in vitro*. However, olaparib-enhanced anti-tumor activity of CAR-T cells *in vivo* might be very complicated.

MDSCs have emerged as important contributors to solid tumor immune evasion. This negative effect has been ascribed to their immunosuppressive roles and their effects on tumor cell invasion and angiogenesis.[33] Tumor-induced MDSCs were associated with poor CAR-T cell efficacy against xenografts *in vivo*, implicating the immunosuppressive solid tumor microenvironment as a modulator of CAR-T cell efficacy.[21] In the study, increased $CD8^+$ T cells and decreased recruitment of MDSCs were detected in tumor tissue of the combination treatment group. Our results showed that more apoptosis of $CD8^+$ T cells and inhibited lytic activity of CAR-T cells

could be induced by co-culture with MDSCs *in vitro*. Thus, more residence of $CD8^+$ T cells in tumor tissue of mice treated with olaparib may be at least partially ascribed to less recruitment of MDSCs. In addition, EGFR*v*III-positive tumor cells treated with olaparib showed a state of senescence, with less cell proliferation. Senescent cells could secret various cytokines and chemokines to recruit immune cells, which might also induce the infiltration of $CD8^+$ T cells into tumor tissue.

Notably, a significant increase in the number of MDSCs was found in tumor tissue in the CAR-T cell treatment group compared with the control, and this correlated with the number of CAR-T cells administered. These results suggested that CAR-T cell administration might induce more recruitment of MDSCs into tumor tissue, and the accumulation of intratumoral MDSCs might contribute to immunosuppression in tumor. The recruitment of MDSCs induced by CAR-T cells to tumor might be affected by complicating factors. It has been reported that a set of tumor-derived microRNAs were elevated in melanoma patients treated with immune checkpoint inhibitors and associated with MDSC infiltration.[34] Moreover, some chemokines, such as CXCL1, could be increased under monoclonal antibody treatment, thereby promoting more MDSC infiltration to the tumor.[35] In this study, the expression of CXCL1, CCL2, and CCL5 were found increased in tumor tissue of E0771EGFR*v*III tumor-bearing mice with a high dose of CAR-T cell treatment (5×10^6), compared with a low dose of CAR-T cell treatment (2×10^6), and these enhanced chemokines induced by CAR-T cells administered might lead to more MDSC recruitment to tumor tissue. It is necessary to do more work to clarify the mechanism of CAR-T cells inducing infiltration of MDSCs in the future.

CAFs are differentiated from quiescent fibroblasts and are associated with increased expression of myofibroblastic markers, such as α-SMA. Multiple studies have shown that CAFs create a microenvironment suitable for cancer cell invasion.[36,37] In this study, CAFs were detected to exist in the tumor tissue of EGFR*v*III-positive tumor-bearing mice. SDF1α, released by CAFs, is probably one of the major chemokines inducing MDSC chemoattractant.[38] Here, in mouse models, the tumor tissue showed less SDF1α expression and consistently less MDSC recruitment in the olaparib combined with CAR-T cell treatment group. Further, our findings demonstrated that SDF1α is the key cytokine in olaparib-reduced MDSC recruitment. The SDF1α/CXCR4 axis plays an important role in promoting the recruitment of MDSCs and the growth and migration of breast cancer cells.[39] With less expression of CXCR4, tumor cells presented less ability for cell proliferation and migration.[40] In this study, CXCR4 expression was significantly decreased in olaparib-treated tumor cells and tumor tissue in the combination treatment group. Additionally, MDSCs treated with olaparib presented a decrease of CXCR4 expression. These results suggested that the SDF1α/CXCR4 axis might play an important role in decreasing the recruitment of MDSCs and tumor cell proliferation in the combination treatment group.

As we know, the tumor microenvironment is generally hypoxic. It has been reported that olaparib could suppress HIF1α expression. Meanwhile, HIF1α could decrease the expression of CXCR4 and SDF1α.[41,42] In this study, we observed reduced SDF1α expression in CAFs under hypoxic conditions when HIF1α was knocked down with siRNA. We concluded that olaparib reduced SDF1α expression in CAFs via downregulation of HIF1α. Meanwhile, in accordance with HIF1α expression, the expression of CXCR4 was decreased in EGFR*v*III-positive tumor cells. In addition, it has been reported that in tumors, PARPi had anti-angiogenesis potential through suppressing VEGFα expression.[28,43] CD31 is known as a platelet-endothelial cell adhesion molecule and is expressed on the surface of vascular endothelial cells. Our results showed that $CD31^+$ cells were decreased in tumor tissue after the combined therapy compared with the CAR-T cell treatment alone (Figures 3J and 4J), suggesting the combined therapy has an anti-angiogenesis capacity. These data demonstrated that olaparib combined with CAR-T cell therapy could not only suppress tumor cell proliferation and MDSC migration via the HIF1α/SDF1α/CXCR4 axis but also inhibit angiogenesis in tumor tissue.

In contrast, many reports on the interaction of PARPi with the immune microenvironment have shown variable results in preclinical breast cancer models. PARPi was shown to promote the expression of PD-L1 in tumor cells, contributing to immunosuppression that was reversed by addition of an anti-PD-L1 antibody.[44] PARPi has also been associated with an increase in T regulatory (T_{reg}) cells.[45] However, we did not observe a significant change in the number of immunosuppressive $CD4^+FoxP3^+$ T_{reg} cells in response to olaparib in our model (data not shown), and the high expression of PD-L1 was also not observed in tumor tissue of the olaparib treatment group or the combination treatment group (data not shown). Stimulator of interferon genes (STING), a major adaptor protein in antiviral innate immune signaling, has been linked to anti-tumor immunity.[46] It has been reported that STING suppresses tumor-induced MDSC differentiation by inhibiting signal transducer and activator of transcription 3 (STAT3) signaling.[47] Recent studies demonstrated that olaparib-induced T cell recruitment is mediated through activation of the cGAS/STING pathway in tumor cells.[13] Whether olaparib-reduced migration of MDSCs is regulated by the STING pathway needs further investigation.

Together, in this study, we identified that olaparib could significantly enhance the anti-tumor efficacy of CAR-T cells in mouse breast cancer xenografts, and the reduced recruitment of MDSCs in the tumor microenvironment was the critical determinant of therapeutic efficacy. Our findings provide a further possibility for clinical trials against breast cancer by combining olaparib with CAR-T cells.

MATERIALS AND METHODS

Cell Lines and Cell Culture

Murine breast cancer cell line E0771 cells (EGFR*v*III, gifted by Dr. Xiang Zhang of Baylor College of Medicine) were cultured in RPMI 1640 medium (GIBCO, USA) with 10% fetal bovine serum (FBS) (Gibco, USA) and 100 U/mL penicillin/streptomycin (Invitrogen, USA). Murine breast cancer cell line 4T1 cells (obtained from the

Cell Bank of the Shanghai Institute of Cell Biology, Chinese Academy of Sciences) were cultured in DMEM (Gibco, USA) with 10% FBS (Gibco, USA) and 100 U/mL penicillin/streptomycin (Invitrogen, USA). 293T packaging cell lines (obtained from the ATCC) were cultured in DMEM (Gibco, USA) with 10% FBS (Gibco, USA). Mouse NIH 3T3 cell lines (obtained from ATCC) were cultured in DMEM (Gibco) with 10% newborn calf serum (NCS) (Gibco, USA) and 100 U/mL penicillin/streptomycin (Invitrogen, USA). All cells were routinely maintained at 37°C in a 5% CO_2 atmosphere incubator. Cell line authentication was not performed. To induce NIH 3T3 cells into CAF cells, NIH 3T3 fibroblasts were incubated with free serum for 24 h, then treated with 2.5 ng/mL TGF-β1 in 10% serum for 24 h.

CAR Design and Generation of CAR-T Cells

The epitope of 806 antibody, EGFR287-302, is only fully exposed on EGFR*v*III or activated EGFR, which makes it a perfect target for CAR-T cell therapy.[18,48] The recombinant murine EGFR*v*III-specific CAR retrovirus was generated as follows. Splenic T cells from C57BL/6 or BALB/c mice were genetically engineered with a 806-28z CAR composed of 806 scFv linked to mouse CD28 and CD3-ζ endodomain. The mouse T cells were isolated from murine spleen using a mouse T cell isolation kit (STEMCELL Technologies, USA) and subsequently stimulated with anti-mouse CD3/28 magnetic beads (Thermo Fisher Scientific, USA) at a bead-to-cell ratio of 1:1 for 24 h. Mouse T cells were cultured in RMPI 1640 with 10% FBS, supplemented with 50 μM/mL β-mercaptoethanol, 100 U/mL penicillin/streptomycin, and 100 U/mL recombinant human IL-2 (Shanghai Huaxin High Biotechnology, China) at 37°C, 5% CO_2 cell incubator.

Animal Experiments

The 4- to 6-week-old C57BL/6 and BALB/c mice were bought from Shanghai Sippr BK laboratory. All animal experiments were performed according to protocols approved by the Shanghai Cancer Institute Experimental Animal Care Commission. 5×10^5 EGFR-*v*III-positive tumor cells were *in situ* inoculated into the fourth inguinal mammary fat pads of C57BL/6 and BABL/c mice. When the tumor volume reached 120 mm^3 (day 14), tumor-bearing mice were randomly grouped (n = 6). Then 50 mg/kg olaparib was intraperitoneally injected for 10 days (discontinuous: 5 days consecutively, 2 days off). Mice intraperitoneally injected with the same volume of PBS were used as control. Then, tumor-bearing mice received tail vein injection of 2×10^6 or 5×10^6 806-28Z CAR-T cells in sterile PBS while the control group received 5×10^6 untransduced (UTD) T cells (day 21). Tumor growth was measured by caliper twice a week. Tumor volumes were calculated using the following formula: Tumor volumes = length × $width^2/2$. Lack of survival was defined as death or tumor size >2,000 mm^3.

Flow Cytometry

To evaluate CAR expression, cells were incubated for an hour with EGFR/biotin-labeled EGFR287-302 expression protein, which was generated by our lab, and then followed by incubation with a PE-conjugated anti-streptavidin antibody for 30 min. To measure the expression of EGFR*v*III on tumor cells, cells were incubated with ch806 antibody for an hour, followed by incubating with fluorescein isothiocyanate (FITC)-conjugated goat anti-human antibody (Invitrogen, USA) for 30 min. The analysis was performed by using a flow cytometer. To analyze the *in vitro* proliferation of CAR-T cells, a CellTrace Violet cell proliferation kit (Thermo Fisher Scientific, USA) was used for labeling of cells to trace multiple generations via dye dilution by flow cytometry. For *in vivo* detection of MDSCs, tumor tissue isolated from tumor-bearing mice was cut into small pieces and resuspended in digestion medium containing collagenase type IV (0.5 mg/mL, Sigma Aldrich, USA), collagenase type I (0.5 mg/mL, Sigma Aldrich, USA), hyaluronidase (0.5 mg/mL, Sigma Aldrich, USA), and DNase I (0.02 mg/mL, StemCell Technologies, USA) for 30 min at 37°C. The suspensions were filtered through a 70 μM Falcon cell strainer, centrifuged, and stained with antibodies against CD45, CD11b, and Gr1 according to the manufacturer's instructions.

In Vitro Cytotoxicity

Cytotoxicity was assessed by the Real Time Cellular Analysis (RTCA). RTCA was detected in the xCELLigence instrument (Agilent Biosciences, USA) according to the manufacturer's instructions. Due to the impact of olaparib on the proliferation of CAR-T cells, target cells were pretreated with 0, 1 μM, or 5 μM olaparib for 24 h. Then the medium of the co-culture of effector and target cells was added with or without olaparib (1 μM or 5 μM). Briefly, E0771, E0771EGFR*v*III, 4T1, and 4T1EGFR*v*III cells (1×10^4) were co-cultured with CAR-T cells with or without olaparib at E/T ratios of 1:3, 1:1, and 3:1 in E-plate at 37°C for 18 h. The percentage of specific cell lysis was calculated using a standard formula provided in the manual.

Enzyme-Linked Immunosorbent Assay (ELISA)

To further assess the function of olaparib on CAR-T cells upon antigen-specific stimulation, CAR-T cells were co-cultured with EGFR-*v*III-positive tumor cells. CAR-T cells or untransduced T (UT) cells were co-cultured with target cells at a 1:1 E/T ratio for 24 h. The release of IFN-γ, IL-2, and granzyme B in cell culture supernatants from activated CAR-T cells were determined by using ELISA kits (MultiSciences Biotechnology, China) according to the manufacturer's instructions.

Immunohistochemistry Staining

Formalin-fixed and paraffin-embedded tumor tissues were examined by immunohistochemistry staining as previously described using anti-CD4 (Abcam, USA), anti-CD8α (Abcam, USA) and anti-CD31 antibody (Abcam, USA).[49] Briefly, the sections were exposed to 3% H_2O_2 in methanol after deparaffinization and rehydration and then blocked with 1% BSA for 30 min at room temperature. After blocking, the sections were incubated with primary antibody overnight at 4°C, followed by incubation with peroxidase-conjugated secondary antibodies (ChemMate DAKO EnVision Detection Kit, Peroxidase/DAB, Rabbit/Mouse) and detection reagents. $CD4^+$ cells and $CD8^+$ cells were quantified by measuring the number of stained cells in sections from three mice in each group. The mean count of the three areas per section was obtained and expressed as the absolute.

Chemotaxis Assay *In Vitro*

In vitro, chemotaxis assay was performed as described previously.[50] For migration, 1×10^6 MDSC cells were added in the upper chamber of a Transwell unit with a 5-μm polycarbonate filter (Corning, USA), and the culture supernatants of CAFs were added in the lower chamber. At 2 h and 6 h of migration, the cells in the lower chamber were counted.

RNA Isolation and Quantitative Reverse Transcriptase PCR (qRT-PCR)

Total RNAs of CAFs and tumor cells were extracted using Trizol reagent. One microgram of total RNA was used for first-strand cDNA synthesis according to the manufacturer's protocol (Promega, USA). The sequences of the qRT-PCR primers are listed in Table S1. Gene expression was analyzed by qRT-PCR using the standard curve method on an ABI 7500 Real-Time PCR System (Applied Biosystems, CA, USA).

RNA Interference and Infection

The siRNAs were designed and synthesized by Sangon Biotech (China). NIH 3T3 cells were transfected at ~50% confluence with siRNAs using Lipofectamine 3000 (Thermo Fisher Scientific, MA, USA). The sequences for successful siRNAs were listed in Table S2. Transfected NIH 3T3 cells with GFP tag negative control siRNA, and the transfection efficiency was 51.2% detected by flow cytometry.

Western Blot Analysis

Cells were washed three times with PBS and lysed in RIPA buffer with a protease inhibitor cocktail. Equal amounts of protein were separated by sodium dodecyl sulfate polyacrylamide gel electrophoresis and transferred to polyvinylidene difluoride membranes (Millipore, USA). The membranes were blocked with 5% non-fat dry milk in PBS containing 0.1% Tween-20 at room temperature for 1 h. Subsequently, the membranes were exposed to the indicated primary antibodies in 5% non-fat dry milk in tris buffered saline Tween (TBST) overnight at 4°C. After washing and incubating with horseradish peroxidase (HRP)-conjugated secondary antibodies for 2 h at room temperature, the membranes were incubated with Pierce ECL Western Blotting Substrate (Thermo Fisher Scientific, USA) as the substrate of HRP and membranes were scanned on film.

MDSC Isolation

The amount of MDSCs was detected to be high in bone marrow (44.3%) and low in spleen (4.11%). MDSCs were isolated via Ly6G magnetic selection from bone marrow of healthy mice by using the myeloid-derived suppressor cell isolation kit (Miltenyi Biotec, USA).

Statistical Analysis

All data are presented as the mean ± SEM. Student's t test was used for two-sample comparisons. One-way analysis of variance (ANOVA) was used for multi-sample comparisons. Tumor growth data were analyzed with two-way ANOVA. All statistical analyses were done using GraphPad Prism 5.0 software. $^*p < 0.05$, $^{**}p < 0.01$, and $^{***}p < 0.001$ were considered statistically significant.

SUPPLEMENTAL INFORMATION

Supplemental Information can be found online at https://doi.org/10.1016/j.ymthe.2020.09.034.

AUTHOR CONTRIBUTIONS

Conception and design: Z.L. Development of methodology: R.S. and H.J. Acquisition of data: R.S. and H.L. Analysis and interpretation of data: R.S. Writing, review, and/or revision of the manuscript: Z.L., H.J., and R.S. Administrative, technical, or material support: J.S., S.D., M.Z., B.S., Y.S., G.D., and H.Z. Study supervision: Z.L.

CONFLICTS OF INTEREST

Z.L. has ownership interests of CAR-T cells relating to this work. The other authors declare no competing financial interests.

ACKNOWLEDGMENTS

This work was supported by National Natural Science Foundation of China (no. 31800659); Shanghai Sailing Program (no. 18YF1422000); the Shanghai Science and Technology Innovation Action Plan (no. 18431902900); the Project of Shanghai Municipal Health Commission (no. 201940118); and the Grant-in-Aid for Young Scientists Foundation of Shanghai Cancer Institute (no. SB18-05).

REFERENCES

1. Porter, D.L., Levine, B.L., Kalos, M., Bagg, A., and June, C.H. (2011). Chimeric antigen receptor-modified T cells in chronic lymphoid leukemia. N. Engl. J. Med. *365*, 725–733.
2. Porter, D.L., Hwang, W.T., Frey, N.V., Lacey, S.F., Shaw, P.A., Loren, A.W., Bagg, A., Marcucci, K.T., Shen, A., Gonzalez, V., et al. (2015). Chimeric antigen receptor T cells persist and induce sustained remissions in relapsed refractory chronic lymphocytic leukemia. Sci. Transl. Med. *7*, 303ra139.
3. Maus, M.V., and June, C.H. (2016). Making Better Chimeric Antigen Receptors for Adoptive T-cell Therapy. Clin. Cancer Res *22*, 1875–1884.
4. Priceman, S.J., Forman, S.J., and Brown, C.E. (2015). Smart CARs engineered for cancer immunotherapy. Curr. Opin. Oncol. *27*, 466–474.
5. Sun, Y. (2016). Tumor microenvironment and cancer therapy resistance. Cancer Lett. *380*, 205–215.
6. Wang, X., Walter, M., Urak, R., Weng, L., Huynh, C., Lim, L., Wong, C.W., Chang, W.C., Thomas, S.H., Sanchez, J.F., et al. (2018). Lenalidomide Enhances the Function of CS1 Chimeric Antigen Receptor-Redirected T Cells Against Multiple Myeloma. Clin. Cancer Res *24*, 106–119.
7. Wu, X., Luo, H., Shi, B., Di, S., Sun, R., Su, J., Liu, Y., Li, H., Jiang, H., and Li, Z. (2019). Combined Antitumor Effects of Sorafenib and GPC3-CAR T Cells in Mouse Models of Hepatocellular Carcinoma. Mol. Ther *27*, 1483–1494.
8. Lord, C.J., and Ashworth, A. (2017). PARP inhibitors: Synthetic lethality in the clinic. Science *355*, 1152–1158.
9. Murai, J., Huang, S.Y., Das, B.B., Renaud, A., Zhang, Y., Doroshow, J.H., Ji, J., Takeda, S., and Pommier, Y. (2012). Trapping of PARP1 and PARP2 by Clinical PARP Inhibitors. Cancer Res. *72*, 5588–5599.
10. Sonnenblick, A., de Azambuja, E., Azim, H.A., Jr., and Piccart, M. (2015). An update on PARP inhibitors–moving to the adjuvant setting. Nat. Rev. Clin. Oncol. *12*, 27–41.
11. Pantelidou, C., Sonzogni, O., De Oliveria Taveira, M., Mehta, A.K., Kothari, A., Wang, D., Visal, T., Li, M.K., Pinto, J., Castrillon, J.A., et al. (2019). PARP Inhibitor Efficacy Depends on $CD8^+$ T-cell Recruitment via Intratumoral STING

Pathway Activation in BRCA-Deficient Models of Triple-Negative Breast Cancer. Cancer Discov. *9*, 722–737.

12. Rajesh, M., Mukhopadhyay, P., Bátkai, S., Godlewski, G., Haskó, G., Liaudet, L., and Pacher, P. (2006). Pharmacological inhibition of poly(ADP-ribose) polymerase inhibits angiogenesis. Biochem. Biophys. Res. Commun. *350*, 352–357.

13. Silva, H.A., Abraúl, E., Raimundo, D., Dias, M.F., Marques, C., Guerra, C., de Oliveira, C.F., and Regateiro, F.J. (2006). Molecular detection of EGFRvIII-positive cells in the peripheral blood of breast cancer patients. Eur. J. Cancer *42*, 2617–2622.

14. Del Vecchio, C.A., Jensen, K.C., Nitta, R.T., Shain, A.H., Giacomini, C.P., and Wong, A.J. (2012). Epidermal growth factor receptor variant III contributes to cancer stem cell phenotypes in invasive breast carcinoma. Cancer Res. *72*, 2657–2671.

15. Yu, H., Gong, X., Luo, X., Han, W., Hong, G., Singh, B., and Tang, C.K. (2008). Co-expression of EGFRvIII with ErbB-2 enhances tumorigenesis: EGFRvIII mediated constitutively activated and sustained signaling pathways, whereas EGF-induced a transient effect on EGFR-mediated signaling pathways. Cancer Biol. Ther. *7*, 1818–1828.

16. Chen, M., Sun, R., Shi, B., Wang, Y., Di, S., Luo, H., Sun, Y., Li, Z., Zhou, M., and Jiang, H. (2019). Antitumor efficacy of chimeric antigen receptor T cells against EGFRvIII-expressing glioblastoma in C57BL/6 mice. Biomed. Pharmacother *113*, 108734.

17. Di, S., Zhou, M., Pan, Z., Sun, R., Chen, M., Jiang, H., Shi, B., Luo, H., and Li, Z. (2019). Combined Adjuvant of Poly I:C Improves Antitumor Effects of CAR-T Cells. Front. Oncol *9*, 241.

18. Curtin, N.J., Drew, Y., and Sharma-Saha, S. (2019). Why BRCA mutations are not tumour-agnostic biomarkers for PARP inhibitor therapy. Nat. Rev. Clin. Oncol *16*, 725–726.

19. LoRusso, P.M., Li, J., Burger, A., Heilbrun, L.K., Sausville, E.A., Boerner, S.A., Smith, D., Pilat, M.J., Zhang, J., Tolaney, S.M., et al. (2016). Phase I Safety, Pharmacokinetic, and Pharmacodynamic Study of the Poly(ADP-ribose) Polymerase (PARP) Inhibitor Veliparib (ABT-888) in Combination with Irinotecan in Patients with Advanced Solid Tumors. Clin. Cancer Res *22*, 3227–3237.

20. Ramalingam, S.S., Blais, N., Mazieres, J., Reck, M., Jones, C.M., Juhasz, E., Urban, L., Orlov, S., Barlesi, F., Kio, E., et al. (2017). Randomized, Placebo-Controlled, Phase II Study of Veliparib in Combination with Carboplatin and Paclitaxel for Advanced/Metastatic Non-Small Cell Lung Cancer. Clin. Cancer Res *23*, 1937–1944.

21. Long, A.H., Highfill, S.L., Cui, Y., Smith, J.P., Walker, A.J., Ramakrishna, S., El-Etriby, R., Galli, S., Tsokos, M.G., Orentas, R.J., and Mackall, C.L. (2016). Reduction of MDSCs with All-trans Retinoic Acid Improves CAR Therapy Efficacy for Sarcomas. Cancer Immunol. Res. *4*, 869–880.

22. Cimen Bozkus, C., Elzey, B.D., Crist, S.A., Ellies, L.G., and Ratliff, T.L. (2015). Expression of Cationic Amino Acid Transporter 2 Is Required for Myeloid-Derived Suppressor Cell-Mediated Control of T Cell Immunity. J. Immunol. *195*, 5237–5250.

23. Allaoui, R., Bergenfelz, C., Mohlin, S., Hagerling, C., Salari, K., Werb, Z., Anderson, R.L., Ethier, S.P., Jirström, K., Påhlman, S., et al. (2016). Cancer-associated fibroblast-secreted CXCL16 attracts monocytes to promote stroma activation in triple-negative breast cancers. Nat. Commun *7*, 13050.

24. Yang, X., Lin, Y., Shi, Y., Li, B., Liu, W., Yin, W., Dang, Y., Chu, Y., Fan, J., and He, R. (2016). FAP Promotes Immunosuppression by Cancer-Associated Fibroblasts in the Tumor Microenvironment via STAT3-CCL2 Signaling. Cancer Res. *76*, 4124–4135.

25. Sun, Y., Mao, X., Fan, C., Liu, C., Guo, A., Guan, S., Jin, Q., Li, B., Yao, F., and Jin, F. (2014). CXCL12-CXCR4 axis promotes the natural selection of breast cancer cell metastasis. Tumour Biol. *35*, 7765–7773.

26. Douglass, S., Meeson, A.P., Overbeck-Zubrzycka, D., Brain, J.G., Bennett, M.R., Lamb, C.A., Lennard, T.W., Browell, D., Ali, S., and Kirby, J.A. (2014). Breast cancer metastasis: demonstration that FOXP3 regulates CXCR4 expression and the response to CXCL12. J. Pathol. *234*, 74–85.

27. Chakravarthy, A., Khan, L., Bensler, N.P., Bose, P., and De Carvalho, D.D. (2018). TGF-β-associated extracellular matrix genes link cancer-associated fibroblasts to immune evasion and immunotherapy failure. Nat. Commun. *9*, 4692.

28. Kovacs, K., Vaczy, A., Fekete, K., Kovari, P., Atlasz, T., Reglodi, D., Gabriel, R., Gallyas, F., and Sumegi, B. (2019). PARP Inhibitor Protects Against Chronic Hypoxia/Reoxygenation-Induced Retinal Injury by Regulation of MAPKs, HIF1α, Nrf2, and NFκB. Invest. Ophthalmol. Vis. Sci. *60*, 1478–1490.

29. O'Rourke, D.M., Nasrallah, M.P., Desai, A., Melenhorst, J.J., Mansfield, K., Morrissette, J.J.D., Martinez-Lage, M., Brem, S., Maloney, E., Shen, A., et al. (2017). A single dose of peripherally infused EGFRvIII-directed CAR T cells mediates antigen loss and induces adaptive resistance in patients with recurrent glioblastoma. Sci. Transl. Med. *9*, eaaa0984.

30. Ahmed, N., Brawley, V.S., Hegde, M., Robertson, C., Ghazi, A., Gerken, C., Liu, E., Dakhova, O., Ashoori, A., Corder, A., et al. (2015). Human Epidermal Growth Factor Receptor 2 (HER2) -Specific Chimeric Antigen Receptor-Modified T Cells for the Immunotherapy of HER2-Positive Sarcoma. J. Clin. Oncol. *33*, 1688–1696.

31. Kim, G., Ison, G., McKee, A.E., Zhang, H., Tang, S., Gwise, T., Sridhara, R., Lee, E., Tzou, A., Philip, R., et al. (2015). FDA Approval Summary: Olaparib Monotherapy in Patients with Deleterious Germline BRCA-Mutated Advanced Ovarian Cancer Treated with Three or More Lines of Chemotherapy. Clin. Cancer Res *21*, 4257–4261.

32. Palácová, M. (2019). Breast Cancer in BRCA1/2 Mutation Carriers - Do We Treat It Differently? Focus on Systemic Therapy for BRCA1/2 Associated Breast Cancer. Klin. Onkol *32* (*Suppl 2*), 24–30.

33. Gabrilovich, D.I., and Nagaraj, S. (2009). Myeloid-derived suppressor cells as regulators of the immune system. Nat. Rev. Immunol. *9*, 162–174.

34. Huber, V., Vallacchi, V., Fleming, V., Hu, X., Cova, A., Dugo, M., Shahaj, E., Sulsenti, R., Vergani, E., Filipazzi, P., et al. (2018). Tumor-derived microRNAs induce myeloid suppressor cells and predict immunotherapy resistance in melanoma. J. Clin. Invest. *128*, 5505–5516.

35. Kumar, V., Donthireddy, L., Marvel, D., Condamine, T., Wang, F., Lavilla-Alonso, S., Hashimoto, A., Vonteddu, P., Behera, R., Goins, M.A., et al. (2017). Cancer-Associated Fibroblasts Neutralize the Anti-tumor Effect of CSF1 Receptor Blockade by Inducing PMN-MDSC Infiltration of Tumors. Cancer Cell *32*, 654–668.e5.

36. Attieh, Y., Clark, A.G., Grass, C., Richon, S., Pocard, M., Mariani, P., Elkhatib, N., Betz, T., Gurchenkov, B., and Vignjevic, D.M. (2017). Cancer-associated fibroblasts lead tumor invasion through integrin-β3-dependent fibronectin assembly. J. Cell Biol. *216*, 3509–3520.

37. Itoh, G., Chida, S., Yanagihara, K., Yashiro, M., Aiba, N., and Tanaka, M. (2017). Cancer-associated fibroblasts induce cancer cell apoptosis that regulates invasion mode of tumours. Oncogene *36*, 4434–4444.

38. Ouyang, L., Chang, W., Fang, B., Qin, J., Qu, X., and Cheng, F. (2016). Estrogen-induced SDF-1alpha production promotes the progression of ER-negative breast cancer via the accumulation of MDSCs in the tumor microenvironment. Sci. Rep *6*, 39541.

39. Jiang, K., Li, J., Zhang, J., Wang, L., Zhang, Q., Ge, J., Guo, Y., Want, B., Huang, Y., Yang, T., et al. (2019). SDF-1/CXCR4 axis facilitates myeloid-derived suppressor cells accumulation in osteosarcoma microenvironment and blunts the response to anti-PD-1 therapy. Int. Immunopharmacol *75*, 105818.

40. Ma, Y., Xia, Z., Ye, C., Lu, C., Zhou, S., Pan, J., Liu, C., Zhang, J., Liu, T., Hu, T., et al. (2019). AGTR1 promotes lymph node metastasis in breast cancer by upregulating CXCR4/SDF-1α and inducing cell migration and invasion. Aging (Albany NY) *11*, 3969–3992.

41. Guan, G., Zhang, Y., Lu, Y., Liu, L., Shi, D., Wen, Y., Yang, L., Ma, Q., Liu, T., Zhu, X., et al. (2015). The HIF-1α/CXCR4 pathway supports hypoxia-induced metastasis of human osteosarcoma cells. Cancer Lett. *357*, 254–264.

42. Xu, W., Xu, R., Li, Z., Wang, Y., and Hu, R. (2019). Hypoxia changes chemotaxis behaviour of mesenchymal stem cells via HIF-1α signalling. J. Cell. Mol. Med. *23*, 1899–1907.

43. Sargazi, S., Saravani, R., Zavar Reza, J., Zarei Jaliani, H., Galavi, H., Moudi, M., and Abtahi, N.A. (2019). Novel Poly(Adenosine Diphosphate-Ribose) Polymerase (PARP) Inhibitor, AZD2461, Down-Regulates VEGF and Induces Apoptosis in Prostate Cancer Cells. Iran. Biomed. J. *23*, 312–323.

44. Jiao, S., Xia, W., Yamaguchi, H., Wei, Y., Chen, M.K., Hsu, J.M., Hsu, J.L., Yu, W.H., Du, Y., Lee, H.H., et al. (2017). PARP Inhibitor Upregulates PD-L1 Expression and Enhances Cancer-Associated Immunosuppression. Clin. Cancer Res *23*, 3711–3720.

45. Huang, J., Wang, L., Cong, Z., Amoozgar, Z., Kiner, E., Xing, D., Orsulic, S., Matulonis, U., and Goldberg, M.S. (2015). The PARP1 inhibitor BMN 673 exhibits

immunoregulatory effects in a Brca1(-/-) murine model of ovarian cancer. Biochem. Biophys. Res. Commun. *463*, 551–556.

46. Corrales, L., McWhirter, S.M., Dubensky, T.W., Jr., and Gajewski, T.F. (2016). The host STING pathway at the interface of cancer and immunity. J. Clin. Invest. *126*, 2404–2411.

47. Zhang, C.X., Ye, S.B., Ni, J.J., Cai, T.T., Liu, Y.N., Huang, D.J., Mai, H.Q., Chen, Q.Y., He, J., Zhang, X.S., et al. (2019). STING signaling remodels the tumor microenvironment by antagonizing myeloid-derived suppressor cell expansion. Cell Death Differ. *26*, 2314–2328.

48. Johns, T.G., Adams, T.E., Cochran, J.R., Hall, N.E., Hoyne, P.A., Olsen, M.J., Kim, Y.S., Rothacker, J., Nice, E.C., Walker, F., et al. (2004). Identification of the epitope for the epidermal growth factor receptor-specific monoclonal antibody 806 reveals that it preferentially recognizes an untethered form of the receptor. J. Biol. Chem. *279*, 30375–30384.

49. Jiang, H., Gao, H., Kong, J., Song, B., Wang, P., Shi, B., Wang, H., and Li, Z. (2018). Selective Targeting of Glioblastoma with EGFRvIII/EGFR Bitargeted Chimeric Antigen Receptor T Cell. Cancer Immunol. Res. *6*, 1314–1326.

50. Li, P., Oh, D.Y., Bandyopadhyay, G., Lagakos, W.S., Talukdar, S., Osborn, O., Johnson, A., Chung, H., Maris, M., Ofrecio, J.M., et al. (2015). LTB4 promotes insulin resistance in obese mice by acting on macrophages, hepatocytes and myocytes. Nat. Med. *21*, 239–247.

YMTHE, Volume *29*

Supplemental Information

Olaparib Suppresses MDSC Recruitment via SDF1α/CXCR4 Axis to Improve the Anti-tumor Efficacy of CAR-T Cells on Breast Cancer in Mice

Ruixin Sun, Hong Luo, Jingwen Su, Shengmeng Di, Min Zhou, Bizhi Shi, Yansha Sun, Guoxiu Du, Honghong Zhang, Hua Jiang, and Zonghai Li

SUPPLEMENTARY MATERIALS AND METHODS

Virus production

Retroviruses were obtained by transfection of 80% confluent 293T cells with 806-28Z CAR and packaging plasmid *p*CL-Eco using poly ethylenimine (PEI). Retroviruses were produced by co-transfection of *p*MSCV-EGFR*v*III together with the packaging plasmid *p*CL-Eco into 80% confluent 293T cells using PEI. Viruses were harvested 48h later and filtered through a 0.45 μm filter unit (Millipore, USA) to remove cell debris.

Murine EGFR*v*III Construction

A murine homolog of the human EGFR*v*III mutation was created by using cDNA sequences spanning the murine EGFR according to report. Briefly, the cDNA sequences cloned into *p*WPT vector to construct the recombinant murine EGFR*v*III. Mouse EGFR*v*III sequences were generated by delete exon 2–7 of mouse EGFR and insert a human EGFR 806 epitope (Amino acids 287–302, CGADSYEMEEDGVRK C) after exon 1. Replication-defective lentiviral vectors containing the recombinant murine EGFR*v*III were then generated by 293T packaging cell lines and used to transfect 4T1 and E0771 cells. Transfected cells were incubated with ch806 Ab followed with FITC-labeled goat anti-human IgG, then positive cells were sorted by flow cytometry. Mouse breast cancer cells E0771EGFR*v*III and 4T1EGFR*v*III cells were constructed by using a lentivirus transfection system.

Proliferation Analysis

Tumor cells and CAR-T cells were plated at 10^4 cells/well in 96-well plates with different concentrations of olaparib or veliparib (0, 0.5 ng/mL, 5 ng/mL, 50 ng/mL, 500 ng/mL, 5 μg/mL). The cell proliferation was analyzed by CCK8 kits at 48h.

Animal experiments

The 4–6 weeks old C57BL/6 mice were bought from Shanghai Sippr BK laboratory animal Co. Ltd. All animal experiments were performed according to protocols approved by the Shanghai Cancer Institute Experimental Animal Care Commission. 5×10^5 EGFR*v*III-positive tumor cells were inoculated into the forth inguinal mammary fat pads of C57BL/6 mice. When the tumor volume reached 120mm^3 (day 14), tumor-bearing mice were randomly grouped (n=6). Mice were administrated with various concentrations of olaparib (10mg/kg, 50mg/kg or 100mg/kg) for 10 days (discontinuous: 5 days consecutively, 2 days off). Then, tumor-bearing mice received tail vein injection of 5×10^6 CAR-T cells in sterile PBS while the control group received 5×10^6 untransduced T (UTD) cells at day 21. Tumor growth was measured twice a week. The tumor volumes were calculated using the following formula: Tumor volumes=length×$width^2$/2. Lack of survival was defined as death or tumor size > 2000 mm^3.

Flow cytometry

To evaluate the impact of olaparib on exhaustion, memory T cells and proliferation of CAR-T cells in the presence of antigen-positive or antigen-negative target cells, EGFR*v*III-positive tumor cells were pre-treated with or without various concentrations of olaparib for 24 h. Then CAR-T cells were labeled with CellTrace Violet, and then, 1×10^5 CellTrace-labeled CAR-T cells were incubated with 1×10^5 EGFR*v*III-positive tumor cells in the presence of various concentrations of olaparib for 24 h. The cells were stained with antibodies against CD3, CD4, CD8, CD44, CD62L, PD1, TIM3 and LAG3 according to the manufacturer's instructions and determined by flow cytometry.

MDSCs Suppression Assays

MDSCs were isolated via Ly6G magnetic selection from bone marrow of healthy mice by using the myeloid-derived suppressor cell isolation kit. To determine whether MDSCs decrease the anti-tumor activity of CAR-T cells *in vitro*, the specific lytic function of CAR-T cells on target cells was examined in the presence of MDSCs. CAR-T cells and target cells were co-cultured at an E:T ratio of 1:1. Isolated MDSCs were added at varying MDSCs:CAR-T cells ratios (1:3, 1:1, 3:1) in E-plate at 37 °C for 18h. Th cytotoxicity was assessed by RTCA.The cytotoxicity of CAR-T cells was analyzed using a standard formula provided in the manual.

Chemotaxis Assay *in vitro*

To determine the effects of olaparib on CAFs-induced chemotaxis of MDSCs, NIH3T3 cells were induced into CAFs by harvested after stimulation with TGFβ for 16 h. The CAFs were treated with 0 or 1μM olaparib for 48h and collected the cell culture supernatants. MDSCs cells (2×10^5) (isolated from bone marrow) were added in the upper chamber and the cell culture supernatants of CAFs from each treatment group were added in the lower chamber. The chamber aperture is 3μm. The cell number in the lower chamber was counted at 2h and 6h. To clarify the effects of olaparib on CXCR4-dependent chemotaxis of MDSCs, MDSCs (2×10^5) (isolated from bone marrow) treated with 0, 1μM olaparib or DMSO for 24 were added in the upper chamber and the cell culture supernatants of CAFs were added in the lower chamber. The chamber aperture is 3μm. The cell number in the lower chamber was counted at 2h and 6h.

***In vivo* and *in vitro* Toxic Effect of olaparib on MDSCs**

To evaluate the direct toxic effect of olaparib on MDSCs, the MDSCs isolated from bone marrow were treated with olaparib *in vitro*. The MDSCs were plated at 10^4 cells/well in 96-well plates with different concentrations of olaparib (0, 0.5 ng/mL, 5 ng/mL, 50 ng/mL, 500 ng/mL and 5 μg/mL). The cell proliferation of MDSCs was analyzed by CCK8 kits at 24h.

The 4–6 weeks old C57BL/6 and BALB/c mice were bought from Shanghai Sippr BK laboratory animal Co. Ltd. All animal experiments were performed according to protocols approved by the Shanghai Cancer Institute Experimental Animal Care Commission. 1×10^6 EGFR*v*III-positive tumor cells were inoculated into the forth inguinal mammary fat pads of C57BL/6 and BABL/c mice. When the tumor volume reached 120mm^3 (day 14), mice were randomly grouped and administrated intraperitoneally with 10mg/kg or 50mg/kg dose of olaparib for 10 days. PBS was served as negative control. After two weeks, the percentages of MDSCs from blood, spleen and bone marrow of mice were determined by flow cytometry.

The separation and culture of tumor-derived CAFs

The EGFR*v*III-positive tumor cells were into mammary fat pads of C57BL/6 and BALB/c mice. After three weeks, mammary tissues near the tumors were isolated, digested with collagenase I, collagenase IV and trypsin, and plated on dishes for culture. Cells grew in two weeks and CAFs were isolated by monoclonal culture.

SUPPLEMENTARY FIGURE AND FIGURE LEGENDS

Fig. S1

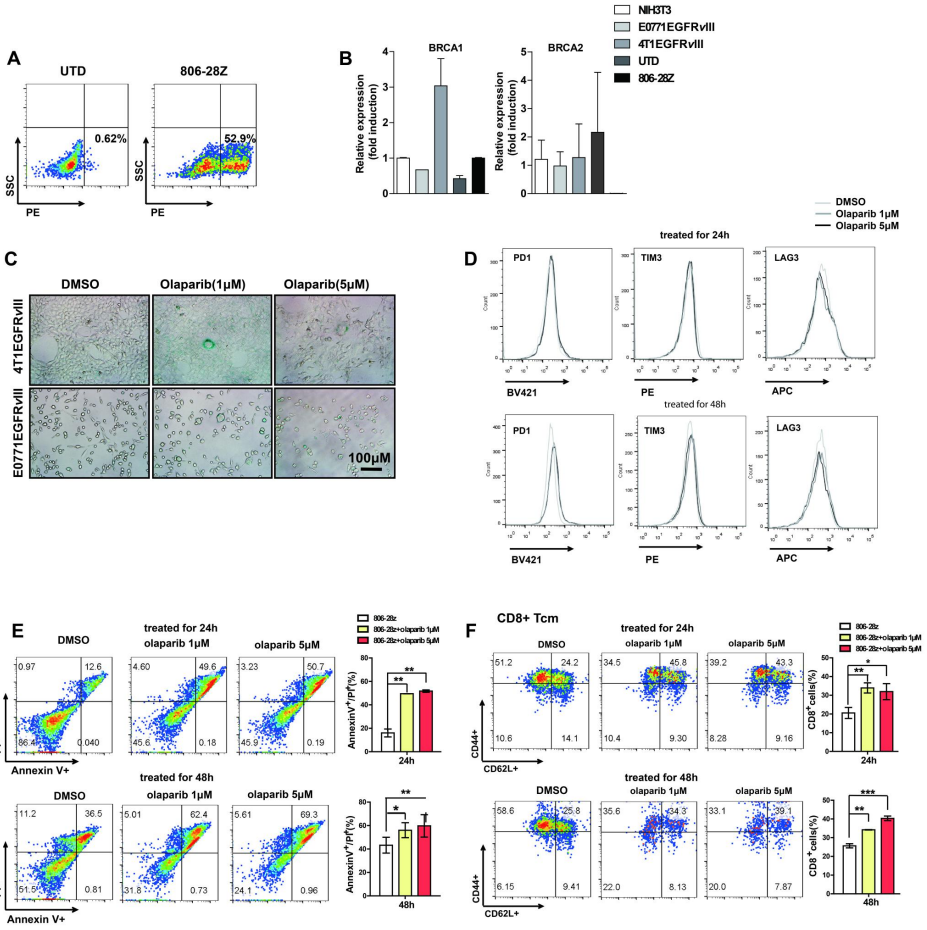

Fig. S1 The effect of olaparib on the phenotype of CAR-T cells

(A) The transduction efficiency of 806-28Z CAR on splenic T cells derived from BABL/c determined by flow cytometry. (B) The mRNA expression of *BRCA1* and *BRCA2* in 4T1EGFR*v*III, E0771EGFR*v*III, NIH3T3, mouse T cells and CAR-T cells. (C) The β-galactosidase staining of E0771EGFR*v*III and 4T1EGFR*v*III cells treated with 0,1μM olaparib or 5μM olaparib for 48h. Scale bars, 100μm. (D) The expression of PD1, TIM3 and LAG3 of CAR-T cells treated with 0, 1μM or 5μM olaparib for 24h or 48h. (E) The representative flow cytometry plots results showing the frequencies of PI^+ and Annexin V^+ CAR-T cells after treated with 0,1 or 5μM olaparib for 24h or 48h. (F) The percentages of CAR-T cells expressing the relevant markers of T_{cm} ($CD44^+CD62L^+$) in $CD8^+$ T cells after treated with 0, 1μM or 5μM olaparib for 24h or 48h, determined by flow cytometry. All data are presented as the mean±SEM of triplicate experiments. **p*<0.05, ***p*<0.01, ****p*<0.001.

Fig. S2

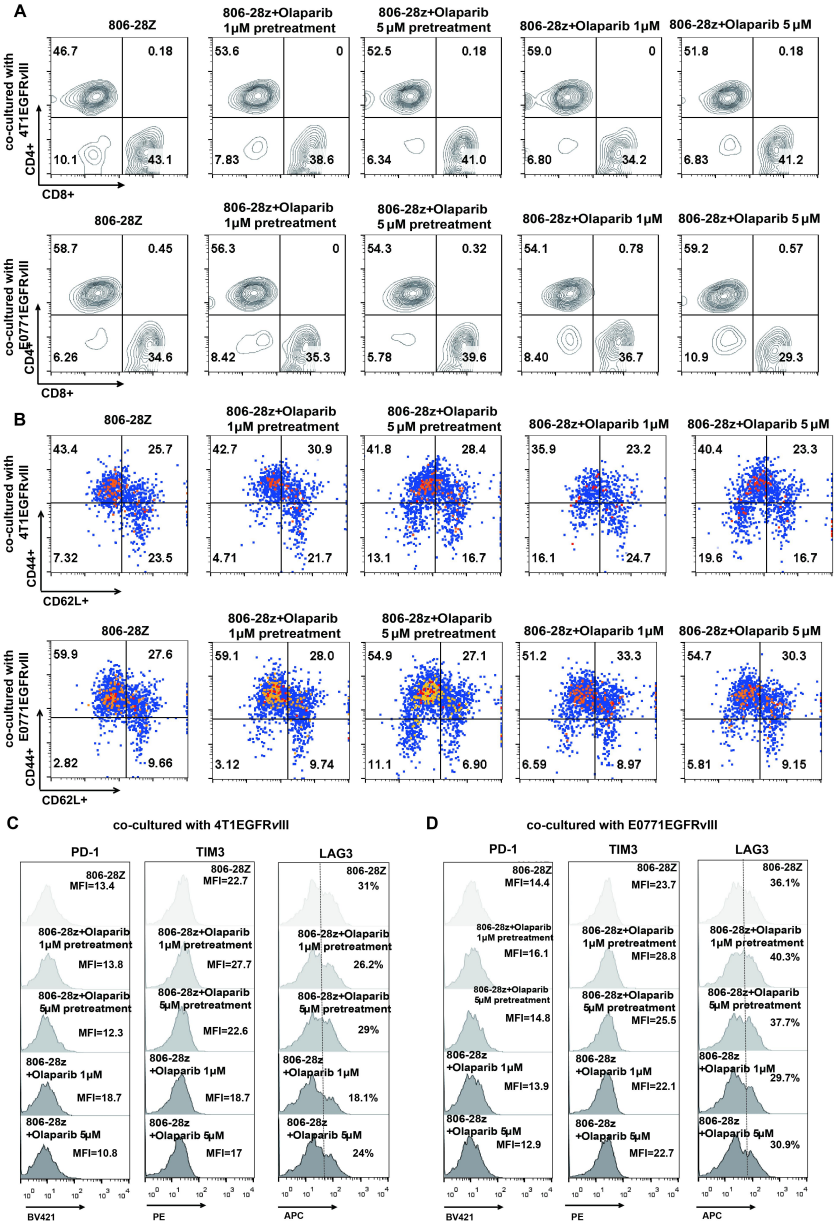

Fig. S2 The effect of olaparib on the phenotype of CAR-T cells in response to antigen stimulation

EGFR*v*III-positive tumor cells were pre-treated with or without various concentrations of olaparib for 24 h. Then, 1×10^5 CellTrace-labeled CAR-T cells were incubated with EGFR*v*III-positive tumor cells at a E/T ratio of 1:1 in the presence of indicated concentrations of olaparib for 24 h. (A) The representative flow cytometry plots results showing the frequencies of $CD4^+$ T and $CD8^+$ T cells in $CD3^+$ CAR-T cells. (B) The percentages of T_{cm} ($CD44^+CD62L^+$) in $CD8^+$ T cells of CAR-T cells in each treatment group. (C) The expression of PD1, TIM3 and LAG3 of CAR-T cells in each treatment group.

Fig. S3

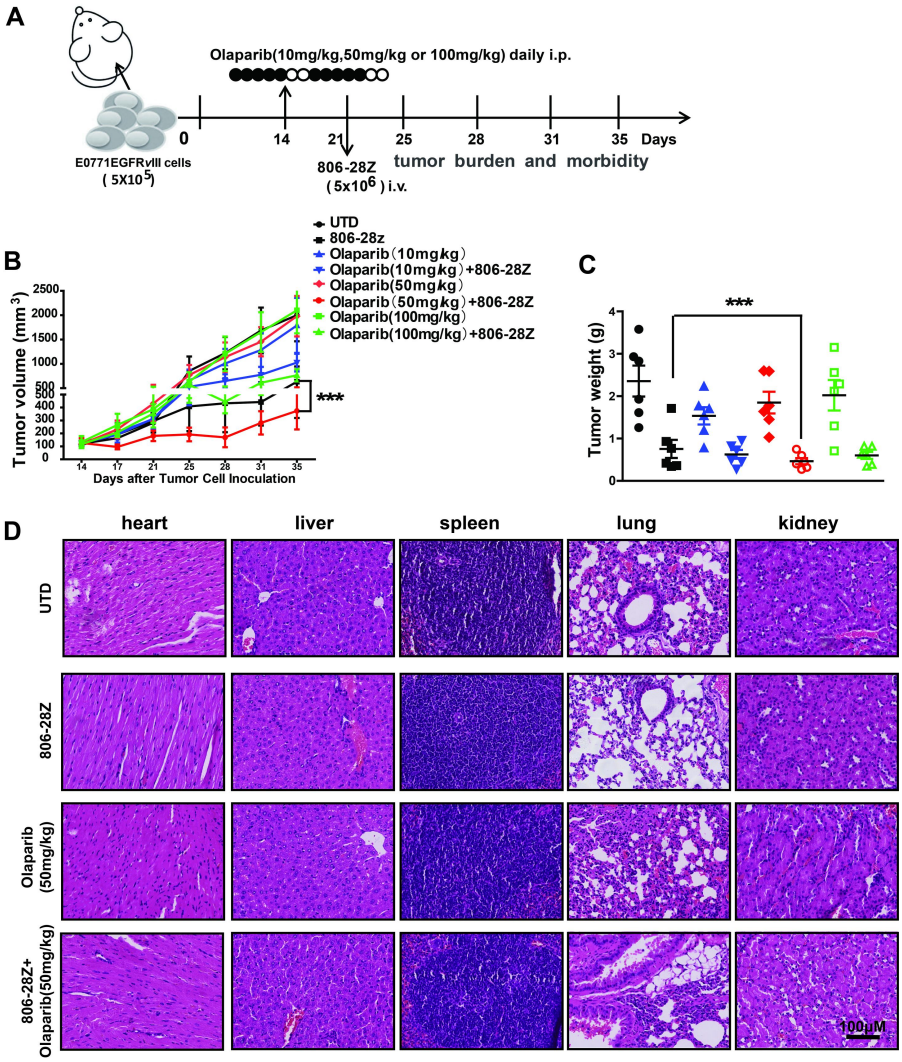

Fig. S3 The anti-tumor activity of different dose of olaparib combined with CAR-T cells in mice bearing E0771EGFR*v*III tumor cells

(A) *In vivo* experimental design. 5×10^5 EGFR*v*III-positive tumor cells were *in situ* inoculated into the forth inguinal mammary fat pads of C57BL/6 mice. Mice were administrated with various concentrations of olaparib (10mg/kg, 50mg/kg or 100mg/kg) for 10 days. Then, tumor-bearing mice received tail vein injection of 5×10^6 CAR-T cells in sterile PBS, while the control group received 5×10^6 UTD cells at day 21. (B) The average tumor growth of each treatment group. (C) The tumor weight of each treatment group. (D) The H&E staining results of heart, liver, spleen, lung and kidney of mice from each group. Scale bars, 100μm. All data are presented as the mean±SEM of triplicate experiments. ***p<0.001

Fig. S4

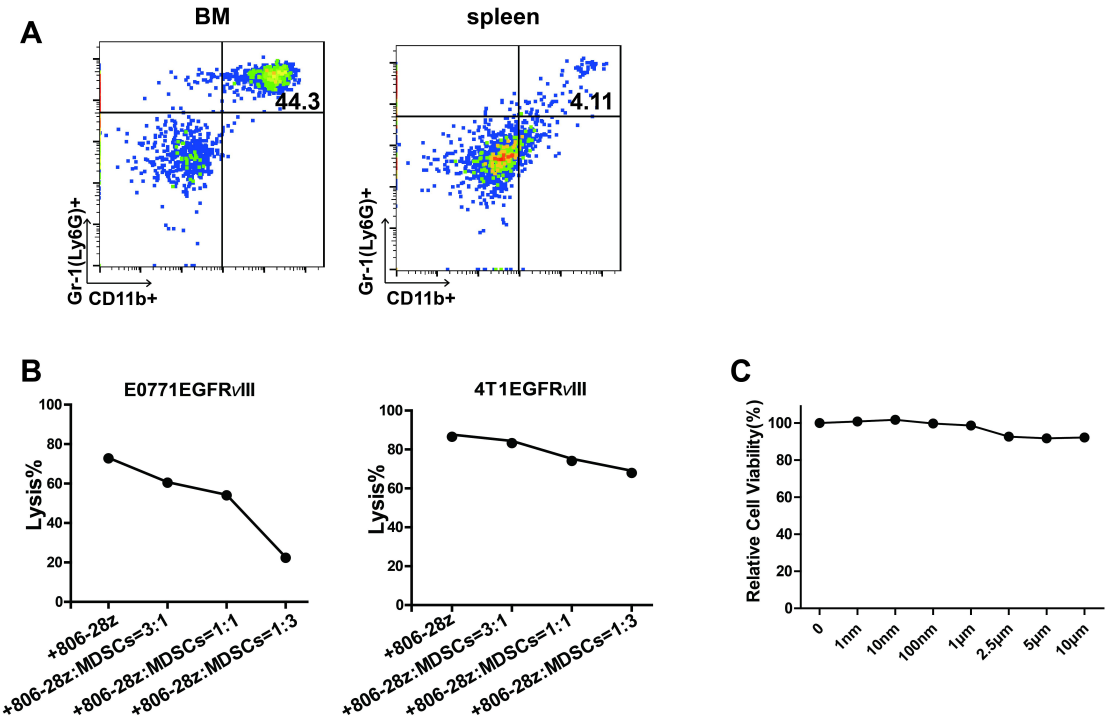

Fig. S4 *In vitro* lytic activity of CAR-T cells against EGFR*v*III-positive tumor cells co-cultured with MDSCs

(A) The representative flow cytometry plots results showing the frequencies of MDSCs ($CD11b^+Gr1^+$ cells) in $CD45^+$ immune cells isolated from bone marrow and spleen. (B) In *vitro* lytic activity of CAR-T cells against E0771EGFR*v*III and 4T1EGFR*v*III cells co-cultured with MDSCs. CAR-T cells and target cells were co-cultured at an E:T ratio of 1:1. Isolated MDSCs were added at different MDSC: CAR-T cell ratios of 1:3, 1:1, 3:1 in E-plate at 37°C for 18 h. The cytotoxicity of CAR-T cells was analyzed using a standard formula provided in the manual. (C) The cytotoxicity of olaparib to MDSCs was shown after treatment with the indicated concentrations of olaparib for 24 h by CCK8.

Fig. S5

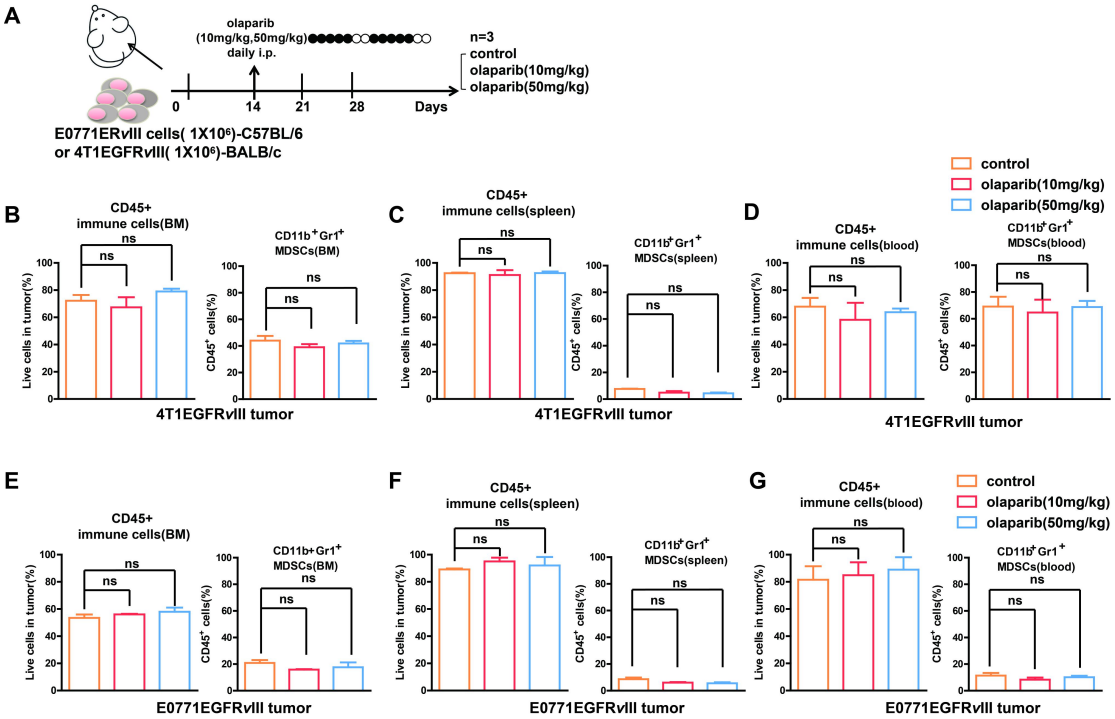

Fig. S5 The direct toxic effect of olaparib on MDSCs *in vivo*

(A) *In vivo* experimental design of EGFR*v*III-positive tumor xenografts. 1×10^6 EGFR*v*III-positive tumor cells were inoculated into the forth inguinal mammary fat pads of C57BL/6 and BABL/c mice. When the tumor volume reached 120mm^3 (day 14), tumor-bearing mice were randomly grouped. Mice were injected with 10mg/kg or 50mg/kg olaparib intraperitoneally for 10 days. (B-D) The quantitation of CD45$^+$ immune cells and MDSCs in various organs: (B) bone marrow, (C) spleen and (D) blood of 4T1EGFR*v*III tumor-bearing mice injected with different dose of olaparib. (E-G) The quantitation of CD45$^+$ immune cells and MDSCs in various organs: (E) bone marrow, (F) spleen and (G) blood of E0771EGFR*v*III tumor-bearing mice injected with different dose of olaparib. All data are presented as the mean±SEM of triplicate experiments. ns, not significant.

Fig. S6

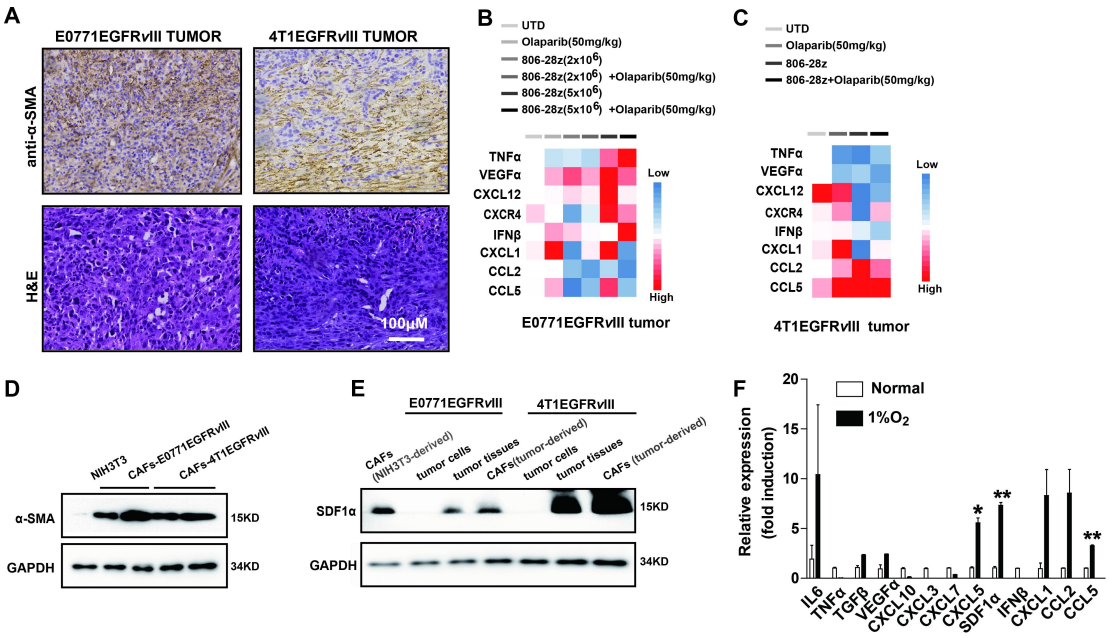

Fig. S6 SDF1α in tumor tissues mainly derived from CAFs

(A) The immunostaining images of α-SMA and H&E staining of tumor tissue from mice bearing EGFR*v*III-positive tumors. Scale bars, 100μm. (B and C) The mRNA expression of cytokines and chemokines in EGFR*v*III-positive tumor tissues of mice from each treatment group. (D) The protein levels of α-SMA and GAPDH were determined in NIH3T3 cells and CAFs isolated from tumor tissue of EGFR*v*III-positive tumor bearing mice. GAPDH served as a loading control. (E) The protein levels of SDF1α and GAPDH were determined in CAFs (induced from NIH3T3 cells), EGFR*v*III-positive tumor cells, EGFR*v*III-positive tumor tissue and CAFs isolated from tumor tissue of EGFR*v*III-positive tumor bearing mice. NIH3T3 cells were starved for 24h and then treated with TGFβ (2.5ng/ml) for 16h to acquire the phenotype of CAFs. GAPDH served as a loading control.

Fig. S7

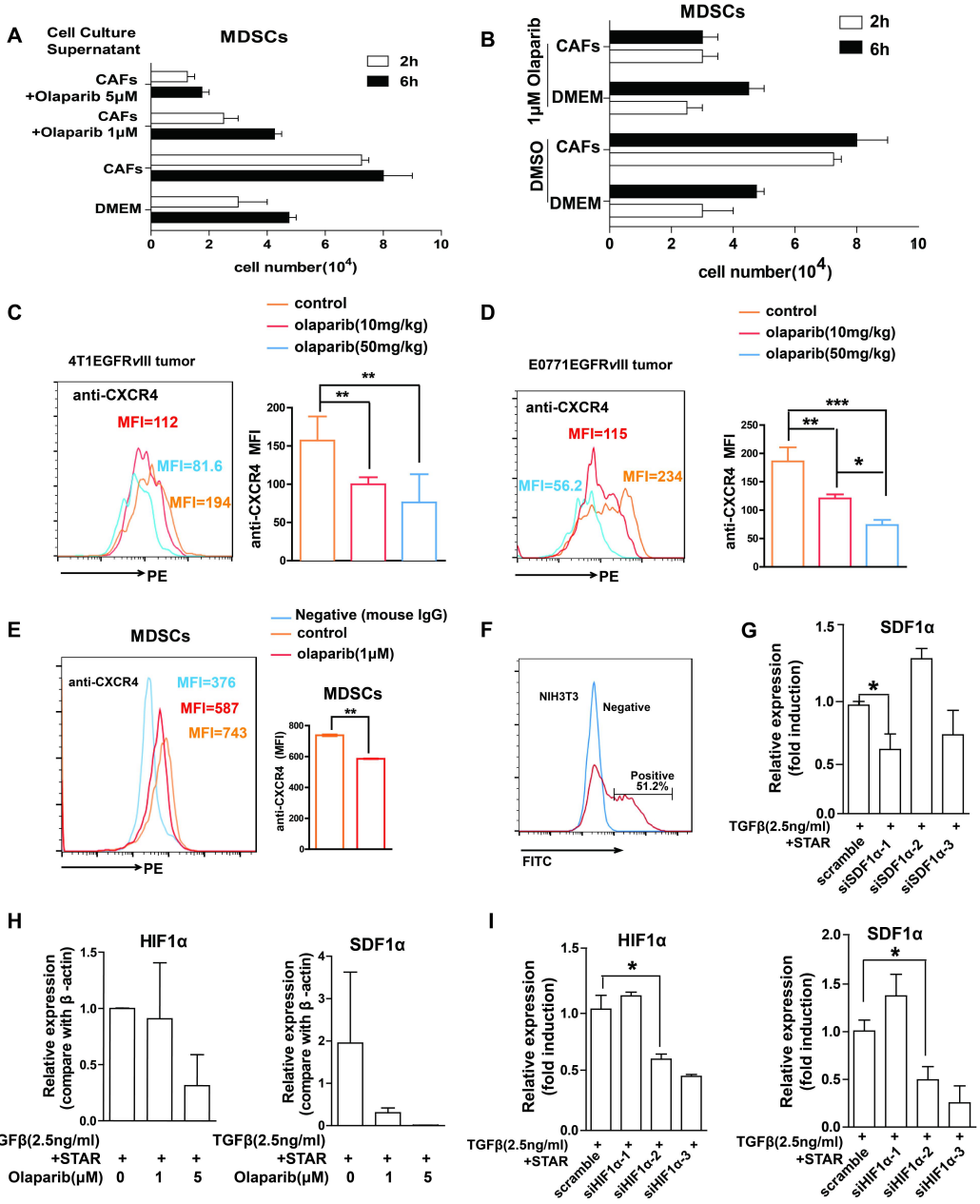

Fig. S7 Effects of olaparib on SDF1α-induced chemotaxis of MDSCs

(A) Effects of olaparib on CAFs-induced chemotaxis of MDSCs. (B) Effects of olaparib on CXCR4-dependent chemotaxis of MDSCs. MDSCs (2×10^5) treated with 1μM olaparib or DMSO for 24 were added in the upper. The cell culture supernatants of CAFs were putted in the lower chamber. The chamber aperture is 3μm. The cell number in the lower chamber was counted at 2h and 6h. (C and D) 1×10^6 EGFR*v*III-positive tumor cells were inoculated into the forth inguinal mammary fat pads of C57BL/6 and BABL/c mice. When the tumor volume reached 120mm^3 (day

14), tumor-bearing mice were randomly grouped (n=3). Then mice were injected with 10mg/kg or 50mg/kg olaparib for 10 days. The expression and quantification results of CXCR4 on MDSCs were determined by flow cytometry in tumor tissue of EGFR*v*III-positive tumor-bearing mice. (E) The expression CXCR4 on the cell surface of MDSCs treated with 1μM olaparib or DMSO (control) for 24h *in vitro* was determined by flow cytometry. Negative: mouse IgG. The numbers above the graphs indicate the MFI of CXCR4. (F) The NIH3T3 cells were transfected with control siRNA (GFP-tag) for 48h. The transfection efficiency of siRNA in NIH3T3 cells was determined by flow cytometry. (G) The CAFs were transfected with siRNA of SDF1α-1, SDF1α-2, SDF1α-3 for 48h. The mRNA expression of SDF1α was determined by Western Blot. (H) The mRNA expression of HIF1α and SDF1α in CAFs treated with 0, 1μM or 5μM olaparib for 48h. (I) The CAFs were transfected with siRNA of HIF1α for 48h. The mRNA expression of HIF1α and SDF1α was determined by RT-qPCR. All data are presented as the mean±SEM of triplicate experiments. *$p<0.05$, **$p<0.01$, ***$p<0.001$.

SUPPLEMENTARY TABLE S1 Primer sequences for various mouse genes for RT-qPCR. Primers were designed using Primer5 software

Gene	**Forward（5'-3'）**	**Reverse（5'-3'）**
UCP1	CCCGACAACTTCCGAAGTGCA	GGAAGCCTGGCCTTCACCTTG
HK1	AGGAAGAACCAACCCACAAAAC	ACCCCAAGGAAACACCACTC
HK2	GGAGGAGATGCGTAATGTGG	TGCCAGGGTTGAGAGAGAG
CPT1b	ACCACAAAGGTCGCTTCTTC	TCTTCATCCAGGGTCACAAAG
CPT2	CTCATCCGCTTTGTTCCTTC	AGTTCATCACGACTGGGTTTG
HSL	TGAGATGGTAACTGTGAGCC	ACTGAGATTGAGGTGCTGTC
ATGL	GAGCCCCGGGGTGGAACAAGAT	AAAAGGTGGTGGGCAGGAGTAAGG
PGC1α	TGCCCCTGCCAGTCACAGGA	GCTCAGCCGAGGACACGAGG
FAS	ACAAACTGCACCCTGACCCAGA	TGCTGGTTGCTGTGCATGGCT
ACC	GAAGTCAGAGCCACGGCACA	GGCAATCTCAGTTCAAGCCAGTC
PKM2	GGAGATGTGGTCATTGTGCTG	AAAGGATAGGGGAGGGGAAG
SREBP-1c	GCTTAGCCTCTACACCAACTGGC	ACAGACTGGTACGGGCCACAAG
PPARα	CAGGAGAGCAGGGATTTGCA	CCTACGCTCAGCCCTCTTCAT
FOXO1	GGACAGCCGCGCAAGACCAG	TTGAATTCTTCCAGCCCGCCGA
GSK-3β	CTGGTGCTGGACTATGTTCC	CGATGGCAGATTCCAAAGGA
iNOS	GTTCTCAGCCCAACAATACAAGA	GTGGACGGGTCGATGTCAC
CCL2	TAAAAACCTGGATCGGAACCAAA	GCATTAGCTTCAGATTTACGGGT
IL-1β	GAAATGCCACCTTTTGACAGTG	TGGATGCTCTCATCAGGACAG
IL-6	GAACAACGATGATGCACTTGC	TCTCTGAAGGACTCTGGCTTTG
TNFα	CCATTCCTGAGTTCTGCAAAGG	AAGTAGGAAGGCCTGAGATCTTATC
CCL2	GCTCAGCCAG ATGCAGTTA	CTGCTGGTGATCCTCTTGTA G
CXCL1	GCTGGGATTCACCTCAAGAA	TGGCTATGAC TTCGGTTTGG
BRCA1	ATGGATTTATCTGCCGTC	CTCAGCAGCTCTTCAGCA
BRCA2	ATGCCCGTTGAATACAAAAG	CTCTGAAAGGCGACTGGT
VEGFα	GGAGACTCTTCGAGGAGCACTT	GGCGATTTAGCAGCAGATATAAGAA
GLUT4	CTTCTTTGAGATTGGCCCTGG	AGGTGAAGATGAAGAAGCCAAGC

FATP1	TGCCTCTGCCTTGATCTTTT	GGAACCGTGGATGAACCTAA
ARG-1	AGTCTGGCAGTTGGAAGCAT	CATCTGGGAACTTTCCTTTC
CCL5	CCCACGTCAAGGAGTATTTC	ACCCTCTATCCTAGCTCATC
18s rRNA	CGGCTACCACATCCAAGGAA	GCTGGAATTACCGCGGCT
SDF1α	GGTTCTTCGAGAGCCACATC	TCTTCAGCCGTGCAACAA

SUPPLEMENTARY TABLE S2 The sequences for siRNA

siRNA	**Sense（5'-3'）**	**Anti-sense（5'-3'）**
siRNA1 HIF1α	GCUCACCAUCAGUUAUUUA TT	UAAAUAACUGAUGGUGAGC TT
siRNA2 HIF1α	CCAUGUGACCAUGAGGAAA TT	UUUCCUCAUGGUCACAUGG TT
siRNA3 HIF1α	GCUGAUUUGUGAACCCAUU TT	AAUGGGUUCACAAAUCAGC TT
siRNA1 SDF1α	GCACGGCUGAAGAACAACA TT	UGUUGUUCUUCAGCCGUGC TT
siRNA2 SDF1α	GAGUACCUGGAGAAAGCUU TT	AAGCUUUCUCCAGGUACUC TT
siRNA3 SDF1α	UCUGCAUCAGUGACGGUAA TT	UUACCGUCACUGAUGCAGA TT
Negative control	UUCUCCGAACGUGUCACGU TT	ACGUGACACGUUCGGAGAA TT